EXPERIMENTAL STUDY ON SINGLE PHASE FLOW AND BOILING HEAT TRANSFER IN MICROCHANNELS AT HIGH FLOW RATES

by
MEHMED RAFET ÖZDEMİR

Submitted to the Graduate School of Engineering and Natural Sciences
in partial fulfillment of
the requirements for the degree of
Master of Science

Sabancı University
July 2010

EXPERIMENTAL STUDY ON SINGLE PHASE FLOW AND BOILING HEAT TRANSFER IN MICROCHANNELS AT HIGH FLOW RATES

APPROVED BY:

Assoc. Prof. Dr. Ali Koşar ……..

(Thesis Supervisor)

Assoc. Prof. Dr. Mahmut Faruk Akşit ..…….....

Assoc. Prof. Dr. Serhat Yeşilyurt …….

Assist. Prof. Dr. Mehmet Yıldız …….....

Assist. Prof. Dr. Kürşat Şendur …….

DATE OF APPROVAL: 22/07/2010

EXPERIMENTAL STUDY ON SINGLE PHASE FLOW AND BOILING HEAT TRANSFER IN MICROCHANNELS AT HIGH FLOW RATES

Mehmed Rafet ÖZDEMİR

Mechatronics Engineering, MSc Thesis, 2010

Thesis Supervisor: Assoc. Prof. Dr. Ali KOŞAR

Keywords: Single Phase Flow in microchannels, Boiling Heat transfer in microchannels, Subcooled flow boiling, High mass flux flow in microchannels

ABSTRACT

With the increasing speed and decreasing size of microprocessors and microchips the sizes of their heat sinks are continuously shrinking from mini size to micro size. The most practical and extensively used micro heat sinks are plain microchannels. They find application in many areas.

The proposed study aims at filling the gap in single-phase fluid flow and boiling heat transfer in microchannels at high mass velocities in the literature. This thesis presents a two-part study. In both part, fluid flow was investigated over a broad range of mass velocity in a microchannel with different inner diameters. De-ionized water was used as working fluid, and the test section was heated by Joule heating. The wall temperatures and pressure drops were measured and processed to obtain heat transfer coefficients, Nusselt numbers, and friction

factors as output. It was found that existing theory for developing flow in conventional scale could fairly predict experimental data on developing flows in microscale for both laminar and turbulent conditions.

In the second part of the study, boiling heat transfer experiments have been carried out for the same microchannel configurations. Heat transfer coefficients and qualities were deduced from local temperature measurements. It was found that high heat removal rates can be achieved at high flow rates under subcooled boiling conditions. It was observed that heat transfer coefficients increase with mass velocity, whereas they decrease with local quality and heat flux. Moreover, experimental heat flux data were compared with partial boiling correlations and fully developed correlations.

YÜKSEK AKIŞ DEBİLERİNDE MİKROKANALLARDA
TEK-FAZLI AKIŞ VE KAYNAMA ISI TRANSFERİ
ÜZERİNE DENEYSEL ÇALIŞMA

Mehmed Rafet ÖZDEMİR

Mekatronik Mühendisliği, Yüksek Lisans Tezi, 2010

Tez Danışmanı: Doç. Dr. Ali KOŞAR

Anahtar Kelimeler: Mikrokanallarda tek-fazlı akış, Mikrokanallarda kaynama ısı transferi, Aşırı soğutulmuş kaynama akışı, Mikrokanallarda yüksek akış debisi

ÖZET

Mikroişlemcilerin ve mikroçiplerin hızlarıyla beraber boyutları da küçüldükçe onları soğutan ısı alıcıları da mini boyuttan mikro boyuta devamlı olarak küçülmeye başlamıştır. Bu mikro ısı alıcılarının en çok kullanılanı düz mikrokanallardır. Düz mikrokanallar birçok alanda uygulama alanı bulmaktadırlar.

Bu çalışma, literatürdeki mikrokanallardaki yüksek akış debilerinde tek-fazlı sıvı akışı ve kaynama ısı transferi alanındaki boşluğu doldurmak için yapılmıştır. Bu tez, iki bölümden oluşmaktadır. Her iki bölümde de, sıvı akışı farklı iç çapı olan mikrokanallarda geniş bir kütle akısı aralığında incelenmiştir. De-ionize su akışkan olarak kullanılmış ve test bölümü elektrikle ısıtılmıştır. Duvar sıcaklıkları ve basınç düşüşleri ölçülerek ısı transferi katsayısını, Nusselt numaralarını ve sürtünme faktörlerini hesaplamak için kullanılmıştır. Makro boyut

için önerilen olgunlaşmakta olan akış teorilerinin hem laminer hem de türbülanslı durumlardaki deneysel sonuçları orta seviyede tahmin ettiği görülmüştür.

Çalışmanın ikinci kısmında ise, aynı mikrokanallar için kaynama ısı transferi deneyleri yapılmıştır. Isı transferi katsayısı ve kütle kalitesi lokal sıcaklık verilerinden ve deneysel koşullardan elde edilmiştir. Aşırı soğutulmuş kaynama şartlarında yüksek akış debilerinde yüksek soğutmanın elde edilebileceği görülmüştür. Ayrıca, ısı transfer katsayısının kütle akısıyla beraber arttığı, lokal kütle kalitesi ve ısı akısıyla beraber azaldığı gözlemlenmiştir. Bununla birlikte deneysel olarak elde edilen ısı akısı verileri kısmi kaynama ve olgunlaşmış aşırı soğutulmuş kaynama korelasyonları ile karşılaştırılmıştır.

Anneme ve Babama…

ACKNOWLEDGEMENTS

I wish to express my sense of appreciate to Dr. Ali KOŞAR for his boundless guidance and advices during my study, and for the long discussions we have made together with him even during his intensive working hours. I am very lucky to have worked with him.

I am grateful to my thesis committee members Dr. Mahmut Faruk AKŞİT, Dr. Serhat YEŞİLYURT, Dr. Mehmet YILDIZ, and Dr. Kürşat ŞENDUR for giving their valuable time commenting on my thesis and their valuable ideas during my study in this university.

I would like to express my thanks to my lab colleagues and lab officers for their superior support and friendship.

This study was supported by TUBITAK (The Scientific and Technological Research Council of Turkey) Support Program for Scientific and Technological Research Projects Grant, 107M514.

Finally, I would like to thank to my family for their love and patience.

TABLE OF CONTENTS

LIST OF TABLES

LIST OF FIGURES

LIST OF SYMBOLS

Latin

A_c	Cross Sectional Area
A_s	Heated Area
C_p	Specific heat at constant pressure
D_i	Inner channel diameter.
D_h	Hydraulic diameter
f	Friction factor
F_{fl}	Fluid surface parameter
f(exp.)	Experimental friction factor
f(theo.)	Theoretical friction factor
G	Mass flux
h_{FG}	Latent heat of vaporization
H_{LO}	Heat transfer coefficient at single phase
h_{sp}	Single-phase heat transfer coefficient
h_{tp}	Two-phase heat transfer coefficient
k_w	Thermal conductivity of the wall
k_f	Thermal conductivity of the fluid
L	Channel Length
L_h	Heated Length
$\dot{m}$	Mass flow rate
MAE	Mean Absolute Error
P	Electrical Power, Pressure
$\dot{q}$	Volumetric heat generation
q''_w	Heat flux
q''_{FC}	Forced convection heat flux
q''_{SB}	Subcooled boiling heat flux
q''_{ONB}	Onset of nucleate boiling heat flux
$\dot{Q_{loss}}$	Heat Loss
R_o	Outer channel radius
R_i	Inner channel radius
T_i	Inlet fluid temperature
T_f	Fluid temperature

T_{sat}	Saturation temperature
$T_{w,i}$	Local inner surface temperature of the microchannel
$T_{w,o}$	Local outer surface temperature of the microchannel
x	Developing length
x_l	Local mass quality
x_{th}	Thermocouple location
w_R	Uncertainty parameter of the result

Greek

ΔP	Pressure Drop
ΔT_{sat}	Difference of inner wall temperature and saturation temperature
μ	Viscosity
ρ	Density

Number Groups

Nu	Nusselt Number
$Nu_{x,H1}$	Thermally developing Nusselt number depending on x
$Nu_{m,H1}$	Mean thermally developing Nusselt number.
Nu_{∞}	Fully developed Nu_H
P_r	Prandtl Number
Re	Reynolds Number
Re_{LO}	Reynolds Number at single phase

Subscripts

f	Fluid
l	Liquid
i	Inner
o	Outer

CHAPTER 1

INTRODUCTION

1.1 Brief Introduction to Microchannels

Since Richard Feynman's motivating speech "There's Plenty of Room at the Bottom" [1] the world has witnessed in its history the most rapid development in technology. Electronic devices have been aggressively miniaturized, so that microelectronics became the most significant technology of the last century. Until recently, the development of non-electronic devices miniaturization remained behind the miniaturization trend in microelectronics. In the 1970s, silicon technology has lead to the fabrication of non-electronic microdevices [2]. This improvement introduced us with MEMS devices which are known as microelectromechanical systems. The research on microchannel cooling originated from the early work of Tuckerman [3], in the 1980s. Extensive literature reviews on heat and fluid flow in microchannels are now available in the literature.

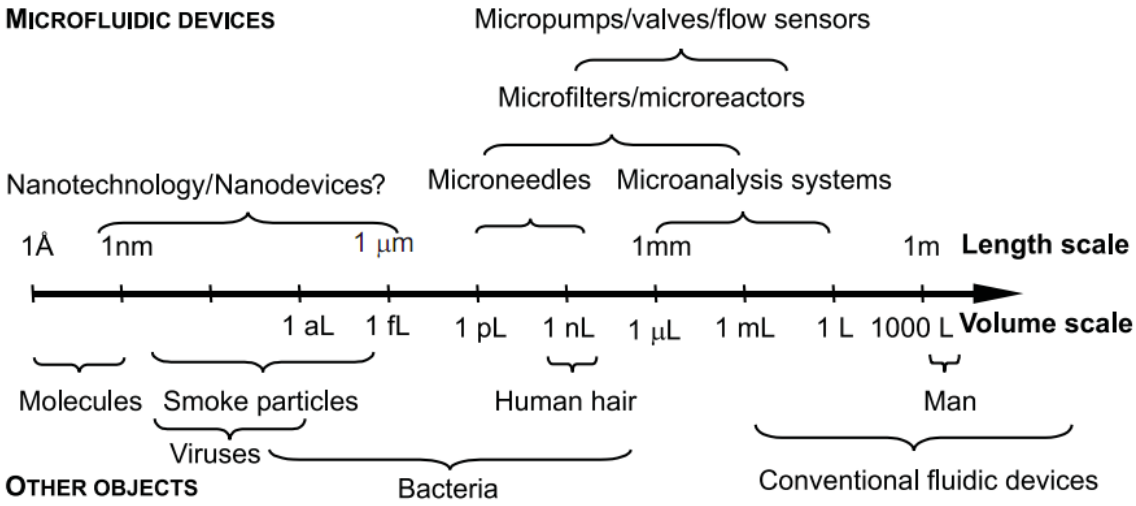

Figure 1.1: Size characteristics of microchannel devices [4]

With the increasing speed and decreasing size of microprocessors and microchips, high heat transfer rates are urgently needed for various applications which attracted the attention of many researchers. Some of the approaches developed over the past decade include the incorporation of densely packed fins [5-6], plate fin surfaces [7], and micro pin-fins in single phase [8-9] and two-phase applications [10]. Recent developments in electronic and integrated circuit technology created a need for higher heat dissipation rates in small sizes. Reducing hydraulic diameters provides a larger surface area per unit volume for a given fluid flow through the channel. However reducing dimensions in order of micrometers in microchannels introduced numerous problems such as high pressure drops, complexity in design, manufacturing and flow instabilities [11-13]. To solve the above issues and convert microchannels into effective heat sinks, some basic issues need to be considered such as cost-effective manufacturing processes, reliable operation, and outstanding thermal and hydraulic performance characteristics for given fluid flow conditions.

1.2 Potential Applications

As mentioned above, with the increasing needs in current microelectromechanical devices, heat sinks are continuously shrinking from mini size to micro size. The most extensively used and practical micro heat sinks are plain microchannels, which find applications in many areas such as in microreactors, fuel cells, drug delivery, micropropulsion, and automotive industry besides electronics cooling. Because of their widespread usage, they attracted the attention of many researchers, which gave rise to many studies on single-phase as well as on flow boiling. Single-phase and two-phase heat transfers have been considered as an important heat removal mechanism for cooling applications in micro scale and were proposed as prominent thermal management solution. New emerging technologies resulting in local heating such as nano-scale plasmonic applications [14-16] and near field radiative energy exchange between objects [17-20] could greatly benefit from single- phase and two-phase heat transfer at high flow rates in micro/nano-scale.

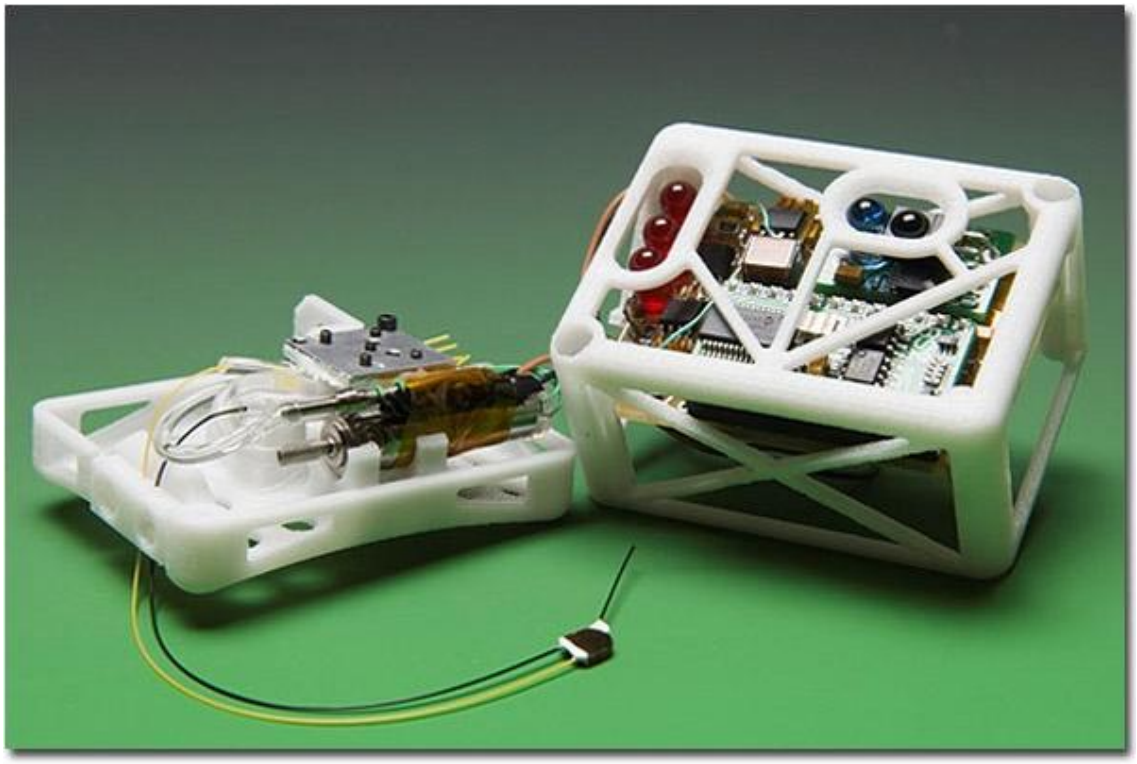

Figure 1.2: Drug delivery test section [21]

As seen in Fig. 1.2, microchannels are also widely used in drug delivery applications. Current efforts in the area of drug delivery include the development of targeted delivery, in which the drug is only active in the target area of the body [22]. Cancerous tissues would be great application for this situation.

Another major industrial success is the invention of MEMS usage for inkjet printer heads in the 1990s [22]. (Fig. 1.3) The printer head consists of microfabricated silicon structure, which serves as an ink storage, a heating element to put the fluid in motion, and a nozzle. The fluid is pushed through the nozzle due to the formation of a bubble near the heating element. This bubble is generated by the vaporization of the ink. The bubble propels the fluid towards the exterior, forming a jet that destabilizes under the action of capillary forces. Droplets created in this way have a size similar to that of the nozzle diameter, which is generally on the order of magnitude 50 μm. These droplets strike the paper, forming the basic spot. Smaller satellite droplets also exist, and form a sort of procession accompanying the principal drop.

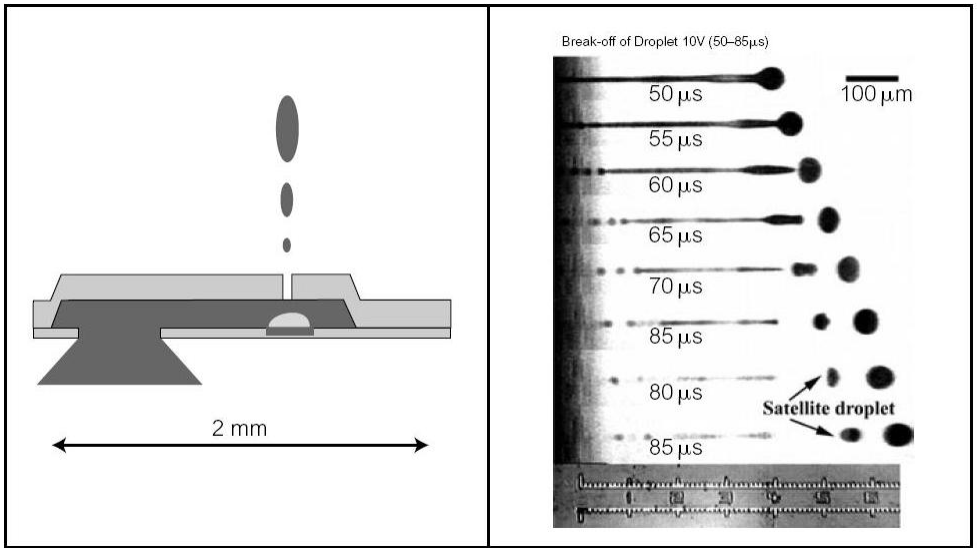

Figure 1.3: A printer head of a inkjet made using MEMS technology [22]

MEMS had been used for airbags activation during the years [22]. (Fig. 1.4) It consists of an integrated system on silicon, which can incorporate both electronic parts and electromechanical parts to detect physical impact. This detection part is in the order of hundred micrometers large and is located in the middle of the chip.

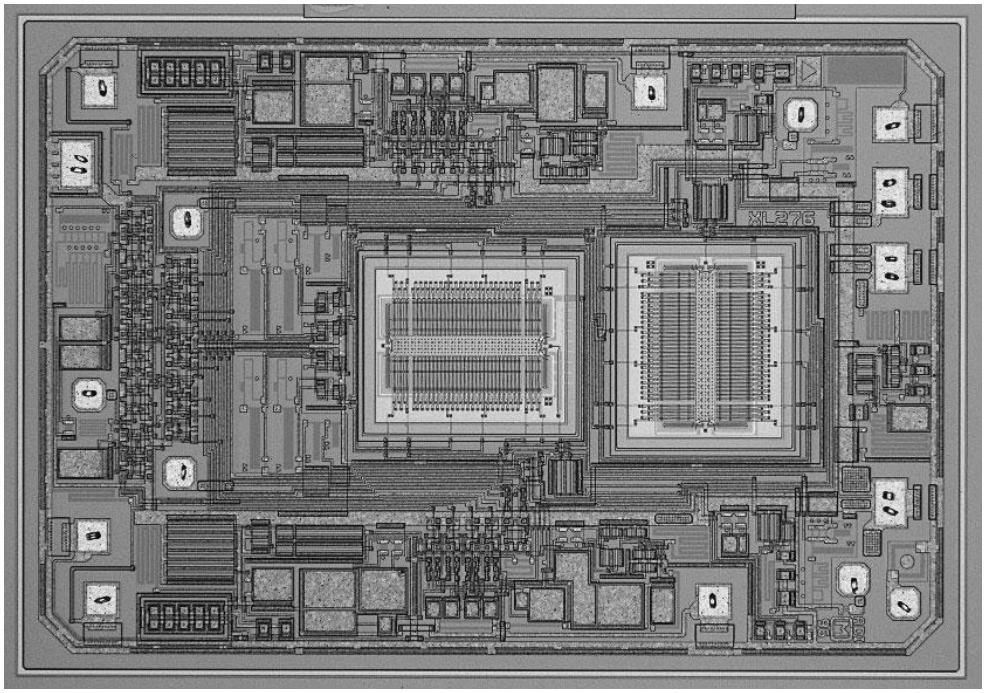

Figure 1.4: Device for the detection and command of airbag activation, based on MEMS technology [23]

As indicated previously, microchannels have numerous applications in the current research and industry. Possible applications are summarized in Table 1.1.

Table 1.1: A list of applications of microchannels [22]

Industry	**Application**
Pharmaceutics	Drug discovery, drug testing, process quality control
Medical	Drug delivery, in vivo diagnostics
Diagnostics (IVD)	Point of care analysis, total analysis systems
Food Industry	Food diagnostics, packaging (smart sensors), functional food testing
Biotechnology	DNA chips, protein chips, cell chips
Chemistry	Lab-on-a-chip concept, microreaction
Process Industry	Process control, profile measurements (arrays of sensors), on-line measurements
Environmental	Soil (also agriculture), water and air quality measurements
Automobile Industry	Fuel Injection, oil quality monitoring, exhaust gas analysis
Consumer Electronics	Ink-jet printers, local cooling of electronics

Nowadays, the market for MEMS technology is estimated to be worth of several tens of billions of dollars [22]. In USA, there existed 1.6 MEMS per person in 2000 on average, and this number is now estimated to be 4 MEMS per person. Today, numerous industries are involved in MEMS technology as shown in Table 1.2. This table is supplied by DARPA group, which consists of 22 companies involved in the field of MEMS (essentially in the United States). The numbers were released in its 2001 annual report [22].

Table 1.2: Markets of the MEMS [22]

Technological Field	Market 2003 ($ Millions)
Inertial measurements	700-1400
Microfluidics and chemical testing/processing	3000-4450
Optical MEMS (MOEMS)	450-950
Pressure Measurement	1100-2150
RF Technology	40-120
Other	1230-2470

1.3 Microfabrication of Microchannels

This section provides brief information about microfabrication of microchannels. The material selection and microfabrication of microchannel devices is important due to their wide thermal and industrial applications. To provide a succesfull microfabrication process flow, parameters should be carefully considered such as material substrate, wafer selection, and selecting appropriate microfabrication technique. With the increasing significance of MEMS technology, polymers have been used more widely than glass materials in microfabrication of microchannels. Silicon is the most preferred material as a substrate. Other materials can be also used as substrate such as metals, copper, steel, quartz, sapphires, and polymers. While deciding on the substrate material checking machinability and compatibility for metal deposition is also essential in addition to the cost of the substrate material. For example, silicon has a high cost but its machinability and compatibility for metal deposition is very good. On the other hand, plastic has a low cost but its machinability and compatibility for metal deposition is poor. A comparison for some substrate materials is given in Table 1.3.

Table 1.3: Substrate materials comparison [4]

Substrate material	Cost	Compatibility for metal deposition	Machinability
Silicon	High	Good	Very good
Plastic	Low	Poor	Poor
Ceramic	Medium	Fair	Poor
Glass	Low	Good	Poor

Another crucial point is wafer cleaning, which should be performed before the substrate deposition to the wafer. The cleaning process is called RCA (Radio Corporation of America) cleaning, which operates at high temperatures and consists of chemical processes such as oxidation and chemical vapor deposition. RCA cleaning process steps can be defined briefly as below:

- Firstly, all organic coatings should be removed in strong oxidants. (Generally mixture of concentrated sulfuric acid and hydrogen peroxide is used.)
- Organic residues should be removed from the wafer.
- Finally, thin oxide layers and ionic contaminants should be removed carefully.

Generally typical IC fabrication processes and particular micromachining processes have been developed for microsystems applications. Main fabrication processes are oxidation, lithography, etching, EDM, and PDMS Molding methods. In the following subsections these methods will be briefly introduced.

1.3.1 Oxidation

As mentioned before, silicon is one of the most preferred materials for substrate selection. The interface between Si and silicon dioxide is very good. In this process, oxide is needed to form barrier for diffusion, to form insulating film, to separate different levels, and to isolate device. There are two types of oxidation: Dry Oxidation, Wet Oxidation. Wet oxidation is faster than dry oxidation. The reason of this solid solubility of (OH) in SiO_2 surface is several orders of magnitude higher than that of O_2, and the diffusion rate of (OH) in SiO_2 is higher because (OH) is smaller compared to O_2 molecule.

1.3.2 Lithography

Lithography is the process of transferring patterns of geometric shapes on a mask to a thin layer of photosensitive material covering the wafer. The whole process must be carried out in an ultra-clean condition (in a clean room). Firstly, patterns are transferred to an imagable photoresist layer. Photoresist is a liquid film that can be spread out onto a substrate, exposed with a desired pattern, and developed into a selectively placed layer for subsequent processing. Overview of the photolithography process is summarized below:

- Surface Preparation
- Coating
- Pre-Bake
- Alignment
- Exposure
- Development
- Post-Bake
- Processing Using the photoresist as masking film
- Stripping
- Post Processing Cleaning (Ashing)

1.3.3 Etching

Etching is the process of transferring the image in mask and photoresist to underlying layer. It removes surface damage after mechanical polishing. This process also helps to show and identify crystal defects. Below parameters should be considered during the process.

- Etch rate
- Etch rate reproducibility
- Etch rate uniformity
- Selectivity (ratio of etch rate of required material over others)
- Surface damage, safety
- Etch anisotropy

a) Wet Etching

Wet etching is the purely chemical which has lack of anisotropy but highly selective process. It results less damage compared to plasma etching. However, process control in wet etching is poor for dimensions < 2μm. Due to surface tension, deep trenches are difficult to etch. It is easy process since requires less expensive equipments.

b) Dry Etching

Dry etching minimizes most of the wet etching problems such as reaching deep trenches and etching for dimensions < 2μm. In addition, process control can be better achieved. It is less sensitive to small changes in temperature. In dry etching, both chemical and physical processes take place.

c) RIE (Reactive Ion Etching)

In RIE, the substrate is placed inside a reactor in which several gases are introduced. Plasma is struck in the gas mixture using an RF power source, breaking the gas molecules into ions. The resulting ions are accelerated, and react at the surface of the material which is being etched. This is known as the chemical part of reactive ion

etching. There is also a physical part which is similar in nature to the sputtering deposition process. If the ions have high enough energy, they can knock atoms out of the material to be etched without a chemical reaction.

d) DRIE (Deep Reactive Ion Etching)

A special subclass of RIE which continues to grow rapidly in popularity is deep RIE (DRIE). In this process, etch depths of hundreds of microns can be achieved with almost vertical sidewalls. Two different gas compositions are alternated in the reactor. The first gas composition creates a polymer on the surface of the substrate, and the second gas composition etches the substrate. The polymer is immediately sputtered away by the physical part of the etching, but only on the horizontal surfaces and not the sidewalls. Since the polymer only dissolves very slowly in the chemical part of the etching, it builds up on the sidewalls and protects them from etching.

Etching aspect ratios of 50 to 100 can be achieved. The process can easily be used to etch completely through as silicon substrate and etch rates are 3-4 times higher than wet etching. It provides high silicon etching rates, good profile control, high selectivity to masking material, and tolerable nonuniformity.

1.3.4 EDM

EDM (Electrical Discharge Machining) is a microfabrication process for microchannels and micro heat sinks. Material is removed from the work piece by series of rapidly recurring current discharges between the two electrodes, separated by a dielectric liquid and subject to an electric voltage. When the distance between the two electrodes is reduced, the intensity of the electric field in the volume between the electrodes becomes greater than the strength of the dielectric, which allows current to flow between the two electrodes. EDM is generally used for precise cutting in microchannel technology.

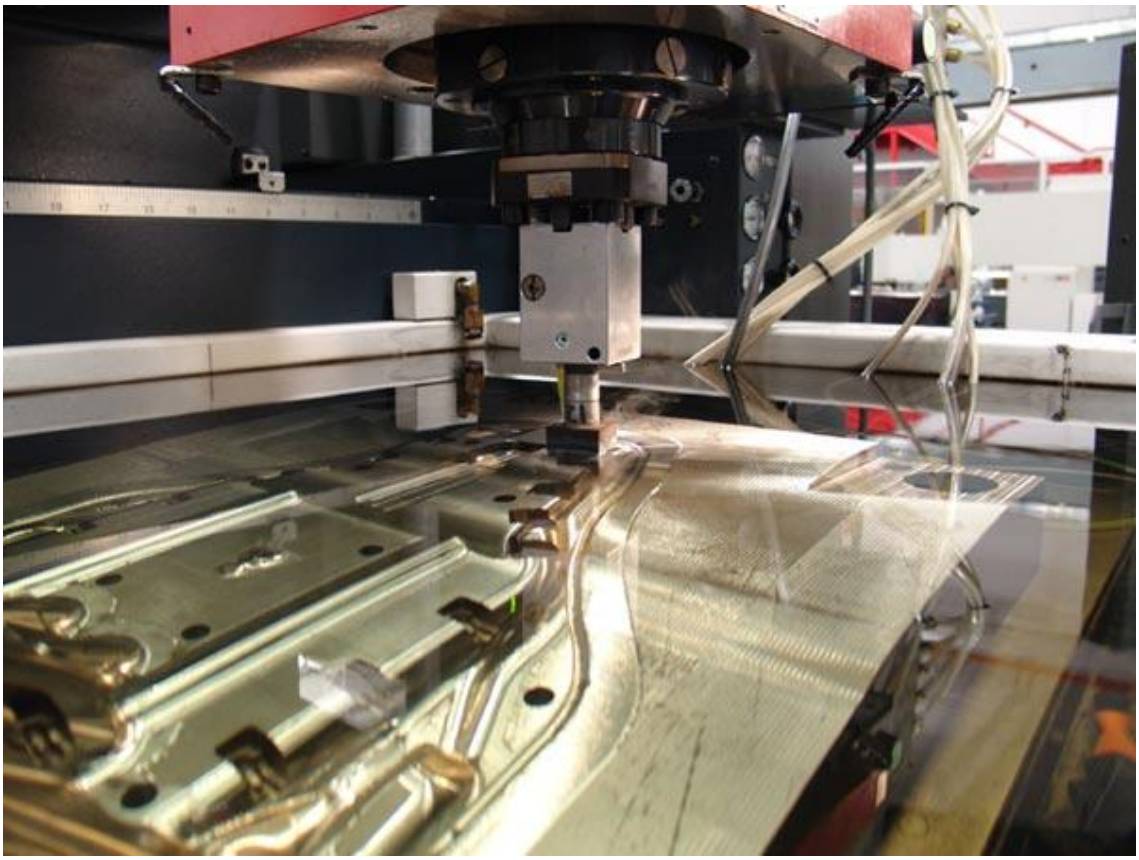

Figure 1.5: EDM Machine [24]

1.3.5 PDMS Molding

Polymethylsiloxan (PDMS) is a material that is optically clear and generally considered to be inert, non-toxic, and non flammable. PDMS molding process is mixing, degasing, and casting PDMS onto a mold. Generally 10:1 mixture of PDMS pre-polymer and a curing agent cast or spin-coated sputtered onto master molds. A weight or clamps (sandwich mold) used for minimizing the PDMS layer on top of master molds. Vacuum pump is used to remove air bubbles from the system. Main advantages of PDMS molding method are:

- There is no need of expensive equipment such as injection molding and hot embossing machines for polymer replication.
- Low temperatures (~65℃) operation is available for curing PDMS.

1.4 Objectives and Major Challenges of This Work

The proposed study involves two parts, which are namely single-phase flow and boiling heat transfer in microchannels at high flow rates. Single-phase flow part aims at filling the gap in heat and fluid flow in microchannels at high mass velocities in the literature. For this purpose, it is intended to investigate single-phase fluid (de-ionized water) flow over a broad range of mass velocity (1300 kg/m^2s-7200 kg/m^2s) in microtubes with inner diameters of ~ 250 μm and ~ 685 μm. Besides comparing the experimental results in fully developed flow to the theory, the focus of this study is on thermally developing flows. It is aimed at measuring wall temperatures, pressure drops and processing to obtain heat transfer coefficients, Nusselt numbers and friction factors.

In boiling heat transfer part of the study, the emphasis is on again high mass fluxes unlike in the literature. Thus, the current study addresses the lack of information about boiling heat transfer at high flow rates and aims at presenting necessary experimental data. For this, an experimental study was conducted at high flow rates in the same microtubes configuration as in the case of single-phase flow part. Mass flux was changed from 1000 kg/m^2s to 7500 kg/m^2s, and two phase heat transfer coefficients and mass qualities were deduced from local temperature measurements. The effect of mass velocity and quality on boiling heat transfer coefficient was investigated.

To meet the objectives presented above the following research plan was implemented:

- Preparation of a leak-proof experimental setup.
- Integration of tested microtubes to the experimental setup.
- Integration of pressure and thermal sensors into the experimental setup at desired locations.
- Installation of Data Acquisition system.
- Development of data acquisition program by using Labview® software.
- Acquiring pressure and temperature data from the system at the desired experimental conditions.
- Reduction of experimental data into single-phase heat transfer coefficients, Nusselt numbers, friction factors, two-phase heat transfer coefficients, and local qualities.

- Comparison of single-phase heat transfer coefficients with existing theory for fully developed and thermally developing conditions.
- Comparison of two-phase heat transfer coefficients with correlations and theory for subcooled flow boiling conditions and partial flow boiling conditions.

1.4.1 Literature Survey for Single-Phase Flow Part

Many experimental studies on microchannels related to the laminar flow [25-27], laminar to turbulent transition [28-38], and turbulent flow [39-42] are present in the literature.

Owhaib et al. [26] experimentally investigated heat transfer characteristics of R 134a through circular microchannels of 1.7, 1.2 and 0.8 mm inner diameters. They compared the results to both the correlations for the heat transfer in macroscale channels and the correlations suggested for microscale geometries. The results showed a good agreement between the classical correlations and the experimental data in the turbulent region. However, none of the correlations suggested for microchannels agreed with the experimental data. In addition to that, they observed that, the heat transfer coefficients were almost identical for three diameters in the laminar regime

Hrnjak et al. [27] focused on investigating fully developed liquid and vapor flow through rectangular microchannels with hydraulic diameters varying from 68.5 to 304.7 μm and with aspect ratios changing from 0.09 to 0.24. They used liquid and vapor R 134a as the testing fluid. During the experiments, they varied Reynolds number from 112 to 9180. They used pressure drop data to find the friction factors in the laminar region, the transition region, and the turbulent region. They concluded that there is no indication of deviation from the existing theory for microchannels.

Morini [30] presented a review on convective heat transfer in microchannels. He analyzed the main experimental results on convective flow in microchannels with regard to the predictive correlations of the existing friction factors, the laminar- to-turbulent transition, and the Nusselt numbers. He showed that a chronological decrease

in the observed deviations is related to the increase of the reliability/accuracy of the recent experimental data.

Celata et al. [61] performed an experimental analysis of the friction factor in a capillary tube having a diameter of 130 μm by using R 114 as the test fluid. They observed the behavior of the laminar-to-turbulent transition for Reynolds numbers ranging between 100 and 8000. Experiments indicate that in the laminar flow regime the friction factors are in good agreement with the conventional theory.

Morini [33] showed that many experimental results on the laminar-to-turbulent transition in microchannels can be explained by using "Obot-Jones model", which is obtained by means of the conventional theory for large size channels. He represented that "Obot-Jones" model helps to understand the role of the cross-section geometry and of the wall roughness on the transition from laminar to turbulent flow through micro-channels. Also even if "Obot-Jones" model is valid for large size channels, he compared the model to the experimental data. The results showed that the model is suitable for micro-channels with a hydraulic diameter greater than 40 μm for predicting the laminar-to-turbulent flow transition.

Rands et al. [38] conducted an experimental study characterizing the laminar-turbulent transition for water flow in circular microtubes. They employed microtubes with diameters in the range of 16.6-32.2 μm over Reynolds numbers 300-3400. They used two independent approaches to identify the transition from laminar to turbulent flow. The first method was determining the transition where friction factor times Reynolds number deviated from the value of 64. The other method was the relations among Reynold number, length, diameter of the tube and Eckert number, which based on the mean temperature rise. They claimed that both methods showed the transition to occur in the Reynolds number range between 2100-2500, which is consistent with macroscale tube flow behavior.

Lorenzini et al. [28] investigated the compressible flow of nitrogen inside circular microchannels of diameters between 26 μm to 508 μm and of different surface roughness for the laminar, transitional, and turbulent flow conditions. They looked at 5000 experimental data. Their data confirmed that in the laminar regime the agreement

with the conventional theory was very good in terms of friction factors for both rough and smooth microtubes. They found that the transitional regime started at Reynolds numbers no smaller than 1800.

Hetsroni et al. [31] showed that the behavior of the flow in micro-channels, at least down to 50 μm diameters, has no differences with the macro-scale flow. For smooth and rough microchannels the transition from laminar to turbulent flow occurred between $1800< R_{cr}<2200$, which was supported by flow visualization and flow resistance data. These studies indicate that the existing theory could provide reasonable predictions for microscale laminar and turbulent flows, while the agreement between the theory and experimental results was not very good for laminar-turbulent flow transition.

There are a few experimental studies present in the literature related to single-phase thermally developing flows in microchannels [32,35, 43-44], because high pressures are typically needed for having thermally developing flows. Thus, high flow rates should be attained to see significant developing effects in microchannels.

Shen et al. [43] conducted experiments to investigate single phase convective heat transfer in a compact heat sink consisting of 26 rectangular microchannels with dimensions of 300 μm in width and 800 μm in depths. They performed tests over Reynolds number range of 162-1257, the inlet liquid temperatures of 30, 50, and 70℃, and the heating powers of 140-450 W. They found that the friction factors and local and average Nusselt numbers significantly departed from those of conventional theories. Additionally, they observed that the hydraulically developed but thermally developing flows have a decreasing Nusselt number trend with the non-dimensional axial distance.

Mishan et al. [44] performed an experimental study in microchannels of D_h = 440 μm and used water as working fluid. Their experimental results about pressure drop and heat transfer confirmed that the conventional theory was applicable for water flow through microchannels if entrance effects are included.

With the change in bulk fluid temperature at high flow rates, the flow may also become turbulent at a certain location downstream the inlet of the channel as a

consequence of fluid property changes. Particularly for short microchannels, developing effects could be sensed at high flow rates and the resulting increased heat transfer characteristics could be greatly exploited in many applications. The present study is aimed to fill the lack of information about single phase flow under these conditions in micro scale. Moreover, with the enhancement in micropumping capabilities, single phase flow could be performed at higher mass velocities so that the gap in this area could be filled with new studies. To investigate single phase flow at high flow rates in micro scale, an experimental study was conducted at high flow rates in micro tubes with a inner diameter of 250 micrometer and 685 micrometer. De-ionized water was used as working fluid, and the test section was heated by Joule heating. Mass flux was changed from 1300 kg/m^{2}s to 7200 kg/m^{2}s, and heat transfer coefficients were deduced from local temperature measurements.

1.4.2 Literature Survey for Boiling Heat Transfer Part

Boiling heat transfer has been considered as an important heat removal mechanism for cooling applications in micro scale and was proposed as a prominent thermal management solution. Many studies were conducted to shed light on boiling heat transfer in microchannels [45-58].

Kosar et al. [45] investigated flow boiling of water in microchannels with a hydraulic diameter of 227 μm possessing 7.5 μm wide reentrant cavities on the side walls. They obtained average two-phase heat transfer coefficients and CHF conditions over a range of heat fluxes (28-445 W/cm^2) and mass velocities (41-302 kg/m^{2}s). They found that high boiling numbers and Reynolds numbers to promoted convective boiling, while nucleate boiling dominated at low Reynolds numbers and Boiling numbers. They also provided a criterion for the transition between nucleate and convective boiling. They showed that existing correlations did not provide satisfactory agreement with heat transfer coefficients but did predict CHF well.

Huh et al. [46] used a rectangular microchannel (D_h=103.5 μm and 133 μm) to perform an experimental study. They studied experimental local boiling heat transfer coefficients, bubble inception, growth, and departure. They performed the tests at mass fluxes of 77.5, 154.9, and 309.8 kg/m^{2}s and heat fluxes of 180-500 kW/m^2. They

observed that in the middle of the test channel nucleate boiling was the dominant heat transfer mechanism. They also observed periodic oscillations of pressure drop particularly at higher mass and heat fluxes.

Lee et al. [47] studied microchannels of different widths (from 102 μm to 997 μm) and of channel depth of 400 μm. They pointed that experimental results allow a critical assessment of the applicability of existing models and correlations in predicting the heat transfer rates and pressure drops in microchannel arrays, and lead to the development of models for predicting the two-phase pressure drop and saturated boiling heat transfer coefficient. The common feature of the performed research is focused on saturated flow boiling at low mass velocities ($G<1000$ kg/m^{2}s). Critical heat flux and boiling instabilities imposed limitation to the extension of micro scale cooling capabilities to higher heat fluxes [49, 50].

Wang et al. [49] carried out a study to investigate stable and unstable flow boiling phenomena in a single microchannel having a hydraulic diameter of 155 μm. They identified stable and unstable flow boiling modes, and flow pattern maps in terms of heat flux, mass flux, and exit vapor quality. They found that unstable flow boiling occurred in the single microchannel if the exit vapors quality $x_e>0.013$.

Bogojevic et al. [50] carried out an experimental study on boiling instabilities in a microchannel silicon heat sink with 40 parallel rectangular microchannels, having a length of 15 mm and a hydraulic diameter of 194 μm. They observed that boiling lead to asymmetrical flow distribution within microchannels that resulted in high temperature non-uniformity and the simultaneously existence of different flow regimes along the transverse direction. They observed two types of two-phase flow instabilities with appreciable pressure and temperature fluctuations, which depended on the heat to mass flux ratio and inlet water temperature. These two types of two-phase flow instabilities were named as high amplitude/low frequency (HALF) and low amplitude/high frequency (LAHF). They also observed that the inlet water subcooling condition affected the magnitudes of the temperature oscillations in two-phase flow instabilities and flow distribution within the microchannels.

Kosar et al. [13] investigated flow boiling under unstable boiling conditions in three different micro-fin pin heat sinks using water and R-123 as working fluids. They used the flow images and FFT (Fast Fourier Transformation) of pressure signals to

explain experimental results. They observed that no significant pressure fluctuations with respect to time averaged pressure drop were evident for the tested micro-pin fin heat sinks before and after flow boiling instability initiates. They recorded a step change in the pressure signals with the inception of unstable boiling. A sharp increase in the magnitude peaks of the FFT profiles was observed in the device operated with R-123, while there was no significant change in the FFT profiles in the devices operated with water.

Due to the increasing trend in critical heat flux and suppression of boiling instabilities with increasing mass velocity flow boiling is becoming more and more attractive at higher mass velocities, where subcooled boiling conditions are expected at high mass velocities. Thus, with the shift from low to high flow rates, a transition in both boiling heat transfer (saturated boiling heat transfer to subcooling boiling heat transfer) and critical heat flux (dryout type critical heat flux to departure from nucleate boiling critical heat flux) from one mechanism to another is likely to occur [51].

However, CHF (Critical Heat Flux) is a mechanism that should be paid attention is subcooled flow boiling. There exist some prediction tools in the literature [52-55]. Lee et al. [54] measured and examined CHF for subcooled flow boiling in mini/micro-channel heat sinks using HFE 7100 as working fluid. They achieved high subcooling by pre-cooling the working fluid. They observed high subcooling was reduced by both bubble departure diameter and void fraction beyond the bubbly regime. They also showed that CHF was triggered by vapor blanket formation along the micro-channel walls. They developed a systematic technique to modify existing CHF correlations to more accurately account for features unique to mini/micro-channel heat sinks. Their technique was shown to be successful at correlating micro-channel heat sink data corresponding to different hydraulic diameters, mass velocities and inlet temperatures.

Few experimental studies are present in the literature related to flow boiling in mini/micro scale at high flow rates and under subcooled flow boiling conditions [56-58]. Haynes et al. [57] examined subcooled flow boiling heat transfer coefficients with tube diameters of 0.92 and 1.95mm. The corresponding heat and mass fluxes were 11-170 kW m^{-2} and 110-1840 kg m^{-2} s^{-1}, respectively. Their Reynolds number range was between 450 and 12000. They showed that the data in the subcooled and saturated

regions are well presented by the simple superposition of convective and nucleate boiling heat transfer mechanisms.

Callizo et al. [58] experimentally investigated subcooled flow boiling heat transfer for refrigerant R-134a in vertical cylindrical tubes with 0.83, 1.22, and 1.70mm internal diameter. They explored the effects of the heat flux, mass flux, inlet subcooling, pressure, and channel diameter on the subcooled boiling heat transfer. They concluded that an increase in the mass flux leads (for early subcooled boiling) to an increase in the heat transfer coefficient.

The literature about subcooled and low quality flow boiling is already present and contains some prediction tools in macro scale [51, 59-60]. However, since scaling laws are not applicable to two-phase and boiling flows [59], there exists a lack of data and information about flow boiling under subcooled boiling and high flow rate conditions in microscale. This thesis addresses to fill the gap in flow boiling under these conditions in micro scale. Moreover, with the enhancement in micropumping capabilities, flow boiling could be performed at higher mass velocities so that high cooling rates (>1000 W/cm^2) could be attained.

To investigate flow boiling at high flow rates and under subcooled conditions in micro scale, an experimental study was conducted at high flow rates in micro tubes. The microtube sizes were used as approximately 250μm and 685μm inner diameters. Deionized water was used as working fluid, and the test section was heated by Joule heating. Mass flux was changed from 1000 kg/m^2s to 7500 kg/m^2s, and heat transfer coefficients were deduced from local temperature measurements. The effects of mass velocity and quality on boiling heat transfer coefficients were investigated. In addition, the potential of reaching high cooling rates was also verified.

CHAPTER 2

EXPERIMENTAL TEST SETUP AND PROCEDURE

2.1 Experimental Test Setup

The experimental setup consists of the test section, a storage cylinder, an Omega® flow meters, pressure sensors and proper tubing, and fittings. Two alligator clips, each 3 mm wide, were attached to the heated length on the microtube surface. They were installed with a prescribed distance (heated length) from each other and were connected to a high current power supply with an adjustable DC current and high power input to provide Joule Heating to the 14.88cm long microtubes of ~ 254µm and ~ 685µm inner diameters. The heated length was adjusted to 5.65 cm.

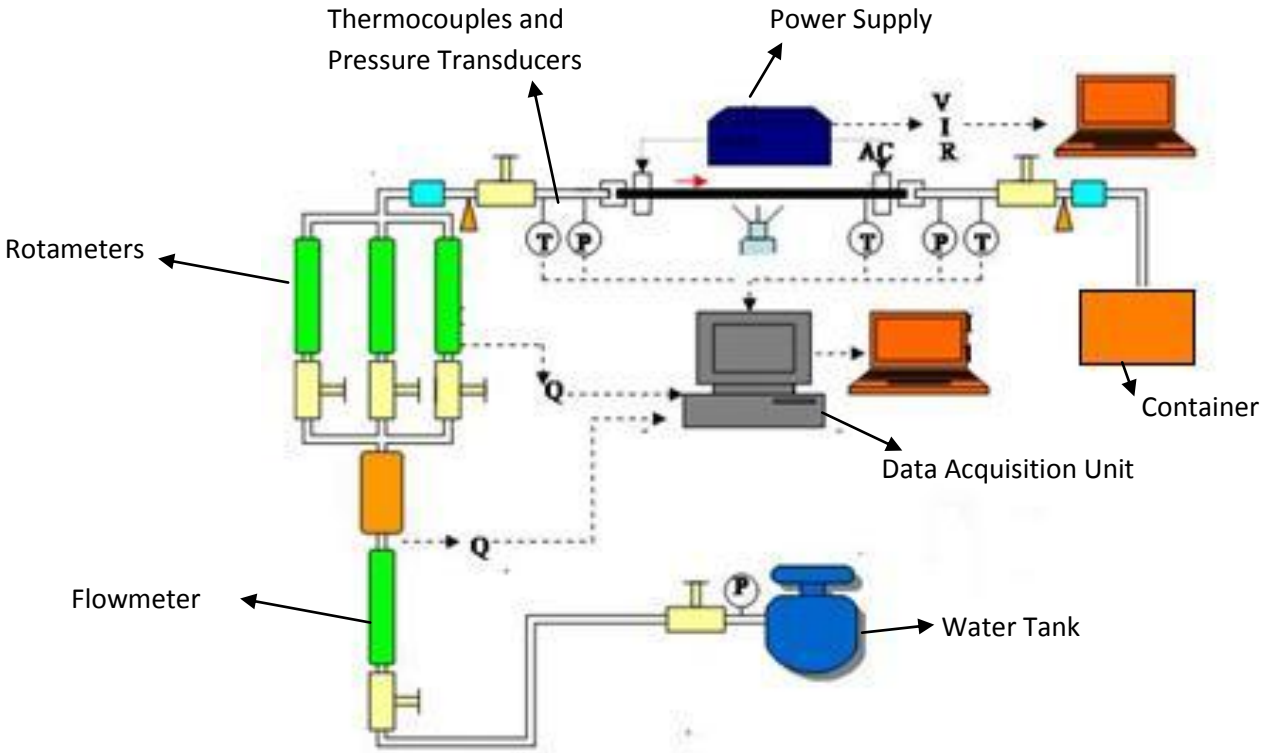

Figure 2.1: Schematic Experimental Test Setup

The sealing between the microtube and the experimental loop was accomplished by Conax® packing glands consisting of a gland body and a sealant. The microtube was connected to the experimental loop from one side, whereas the other end was exposed to the atmosphere to ensure atmospheric conditions at the exit. To measure local temperatures, three thin Omega® thermocouple wires (~ 76 μm thick) was carefully installed to microtube surface at desired locations using Omega® Bond. Thermocouples were located at x_{th1} = 1.82 cm, x_{th2} = 3.32 cm, and x_{th3} = 4.82cm over the heated length of 5.65cm.

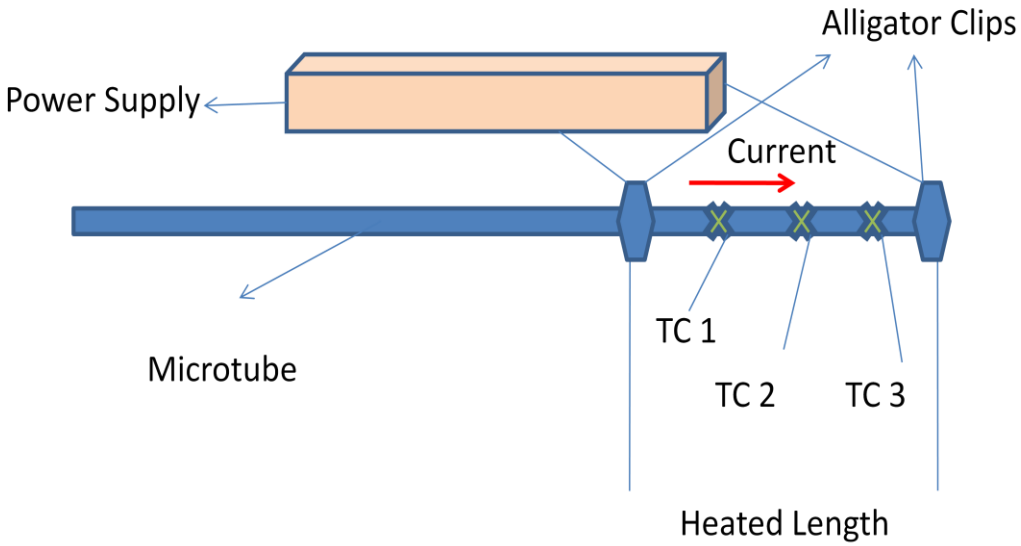

Figure 2.2: Test Section Scheme

One additional Omega® thermocouple was installed to upstream the inlet of the microtube to monitor the bulk temperatures at the inlet. Inlet pressures were measured via Omega® pressure transducers with a 0 to 100 psi gauge pressure range. Flow rate data was obtained together with the voltage, current, and wall/fluid temperetaures, which were acquired through a LabView® interface with time and were transferred to a spreedsheat file for data reduction.

2.2 Experimental Procedure

The de-ionized water flow rate was fixed at the desired value by adjusting the pressure difference between the inlet and exit. It was made sure that temperatures and pressure values obtained from the Labview® interface did not significantly change with time so that experiments could be conducted after steady flow conditions were reached.

For the diabatic tests, the power was increased in ~0.3 Ampere increments. The current/voltage, inlet pressures and wall temperatures were acquired by acquisition rates of 100 data/s and were averaged over time once steady state was reached. This procedure was repeated for different flow rates.

To estimate small heat losses, electrical power was applied to the test section before any fluid flow and experiment. The temperature difference between the ambient and the test section was recorded along with the corresponding power at steady state so that the power could be found as a function of surface temperature to calculate the heat loss ($\dot{Q_{loss}}$) associated with each experimental data point.

2.3 Data Reduction

In this section, equations and correlations which were used to reduce experimental data to the analytical results will be introduced. The data obtained from the voltage, current, flow rate, temperature, and pressure measurements were used to obtain the friction factors, single-phase heat transfer coefficients, Nusselt numbers, two-phase heat transfer coefficients, and local qualities.

The friction factor, f is obtained from adiabatic tests and is given by:

$$f = \frac{2d_i \Delta P \rho_f}{LG^2} \tag{2.1}$$

where d_i is inner diameter of the channel, ΔP is pressure drop, ρ_f is density of the working fluid, L is length of the channel, and G is mass velocity. Using the above

expression, f was evaluated for various mass velocities so that the change in f with Reynolds number was obtained. Reynolds number was expressed as:

$$\mathrm{Re} = \frac{Gd_i}{\mu} \tag{2.2}$$

where d_i is inner diameter of the channel, G is mass velocity, and μ is viscosity of the fluid.

$$G = \frac{\dot{m}}{A_c} \tag{2.3}$$

where $\dot{m}$ is mass flow rate, and A_c is cross sectional area of the channel. For diabatic tests, the electrical input power and resistance were calculated using the measured voltage and current values. Assuming 1-D steady state heat conduction with uniform heat generation, the local inner surface temperature of the microchannel, $T_{w,i}$ is expressed in terms of the measured local outer surface temperature, $T_{w,o}$ as:

$$T_{w,i} = T_{w,o} + \frac{\dot{q}}{4k_w}(r_o^2 - r_i^2) - \frac{\dot{q}}{2k_w} r_o^2 \log(\frac{r_o}{r_i}) \tag{2.4}$$

where k_w is heat thermal conductivity of the wall, r_o is outer radius of the channel, r_i is inner radius of the channel, and $\dot{q}$ is the volumetric heat generation and expressed as a function of net power, inner channel radius, outer channel radius, and heated length as:

$$\dot{q} = \frac{(P - \dot{Q}_{loss})}{\pi(r_o^2 - r_i^2)L_h} \tag{2.5}$$

For single-phase flow, the single-phase heat transfer coefficient is obtained using the inner wall temperature and the net power:

$$h_{sp} = \frac{(P - \dot{Q}_{loss})x_{th}}{A_s(T_{w,i} - T_f)L_h} \tag{2.6}$$

where P is electrical power, $\dot{Q}_{loss}$ is heat loss, x_{th} is location of thermocouple, $T_{w,i}$ is inner wall temperature, T_f is fluid temperature, L_h is heated length, and A_s is inner surface area which is expressed as:

$$A_s = \pi d_i L_h \tag{2.7}$$

where d_i is channel inner diameter, and L_h is heated length. Fluid temperatures are deduced from energy balance:

$$T_f = T_i + \frac{(P - \dot{Q}_{loss}) x_{th}}{\dot{m} c_p L_h} \tag{2.8}$$

where T_i is inlet temperature, P is electrical power, $\dot{Q}_{loss}$ is heat loss, x_{th} is location of thermocouple, $\dot{m}$ is mass flow rate, c_p is specific heat, and L_h is heated length. The Nusselt number is calculated using the average heat transfer coefficient obtained from Eq. (2.6) as:

$$Nu = \frac{h_{sp} d_i}{k_f} \tag{2.9}$$

where h_{sp} is single-phase heat transfer coefficient, d_i is inner diameter of the channel, and k_f is thermal conductivity of the fluid. EES® Software is used to reduce the experimental data to the desired above mentioned parameters in the current study. Since fluid flows should be mostly considered as thermally developing flows under the conditions of the present study thermally developing flow correlations, which were proposed by Shah and London [62] for laminar flows, are suitable to be used for the comparison with the experimental data. Thus, they could be used for predicting the experimental data (under laminar conditions):

$$Nu_{x,H1} = 0.517(f.\mathrm{Re})^{1/3}(x^*)^{-1/3} \tag{2.10}$$

$$Nu_{m,H1} = 0.775(f.\mathrm{Re})^{1/3}(x^*)^{-1/3} \tag{2.11}$$

where f is friction factor and x* can be defined as follow;

$$x^* = \frac{x}{D_h \,\mathrm{Re}\,\mathrm{Pr}} \tag{2.12}$$

where x is developing length and D_h is hydraulic diameter of the channel. For turbulent flows, the following correlations, which have been proposed by Bhatti and Shah [62], have been used for thermally developing flows:

$$\frac{Nu_x}{Nu_\infty} = 1 + \frac{C_6}{10(\frac{x}{D_h})} \tag{2.13}$$

$$\frac{Nu_m}{Nu_\infty} = 1 + \frac{C_6}{(\frac{x}{D_h})} \tag{2.14}$$

where Nu_x is thermally developing Nusselt number depending on x, Nu_m is mean thermally developing Nusselt number, x is developing length, D_h is hydraulic diameter, and Nu_∞ is fully developed Nusselt number. The factor C_6 can be calculated as follow;

$$C_6 = \frac{(\frac{x}{D_h})^{0.1}}{\Pr^{1/6}}(0.68 + \frac{3000}{\mathrm{Re}^{0.81}}) \tag{2.15}$$

where x is developing length, D_h is hydraulic diameter. Nu_∞ in the above equations is the fully developed Nusselt number for thermally developing flows [62] and is expressed as:

$$Nu_\infty = 0.024(\mathrm{Re}^{0.8})\,\Pr^{0.4} \tag{2.16}$$

For boiling conditions, the two-phase heat transfer coefficient was obtained using the inner wall temperature and the net power:

$$h_{tp} = \frac{(P - \dot{Q}_{loss})}{\pi d_i L_h (T_{w,i} - T_{sat})} \tag{2.17}$$

where h_{tp} is two-phase heat transfer coefficient, P is electrical power, $\dot{Q}_{loss}$ is heat loss, d_i is inner diameter of the channel, L_h is heated length, $T_{w,i}$ is inner wall temperature, and T_{sat} is saturation temperature. Local quality was deduced based on energy balance:

$$x_l = \frac{\frac{(P - \dot{Q}_{loss})x_{th}}{L_h} - \dot{m}c_p(T_{sat} - T_i)}{\dot{m}h_{FG}} \tag{2.18}$$

where P is electrical power, $\dot{Q}_{loss}$ is heat loss, x_{th} is thermocouple location, $\dot{m}$ is mass flow rate, c_p is specific heat, T_{sat} is saturation temperature, T_i is inlet temperature, and h_{FG} is latent heat of vaporization. Some subcooled flow boiling correlations are present in the literature. Kandlikar et al. [60] proposed following correlations for subcooled flow boiling, where $q_w^{"}$ is in MW/m^2 and ΔT_{sat} is in K.

$$q_w^{"} = [1058(Gh_{FG})^{-0.7} F_{fl} H_{LO} (T_w - T_{sat})]^{3.33} \tag{2.19}$$

where G is mass flux, h_{FG} is latent heat of vaporization, T_w is wall temperature, T_{sat} is saturation temperature, and F_{fl} is fluid – surface parameter that can be used 1 for any fluid with stainless steel. To calculate H_{LO}, Gnielinski [60] correlation, which is applicable over the range $0.5<Pr_l<2000$ and $2300<Re_{LO}<10^4$, can be used:

$$Nu_{LO}^{*} = \frac{(\mathrm{Re}_{LO} - 1000)(f/2)\,\mathrm{Pr}_l}{[1 + 12.7(\mathrm{Pr}_l^{2/3} - 1)(f/2)^{0.5}]} \tag{2.20}$$

while the correlation of Petukhov and Popov [60] can also be used for the ranges of $0.5<Pr_l<2000$ and $10^4<Re_{LO}<5x10^6$:

$$Nu_{LO}^{*} = \frac{(\mathrm{Re}_{LO})(f/2)\,\mathrm{Pr}_l}{[1 + 12.7(\mathrm{Pr}_l^{2/3} - 1)(f/2)^{0.5}]} \tag{2.21}$$

where f can be calculated as follow:

$$f = (1.58 \ln(\mathrm{Re}_{LO}) - 3.28)^{-2} \tag{2.22}$$

By using equations 2.19, 2.20, 2.21, and 2.22, H_{LO} can be calculated using the following equation:

$$H_{LO} = Nu_{LO}^{*} \left(\frac{k_f}{d_i}\right) \tag{2.23}$$

Bergles et al. [60] proposed the following correlation for the heat flux in partial boiling:

$$q_w^{"} = q_{FC}^{"} \left[1 + \left(\frac{q_{SB}^{"}}{q_{FC}^{"}} - \frac{q_{ONB}^{"}}{q_{FC}^{"}}\right)^2\right]^{1/2} \tag{2.24}$$

where q''_{FC} is the forced convection heat flux, and found using equation 2.25 with H_{LO} representing the single-phase liquid forced convection heat transfer coefficient. The parameter q''_{SB} is the subcooled boiling correlation, which can be found from equation 2.19. q''_{ONB} is the onset of nucleate boiling which is expressed as:

$$q''_{FC} = H_{LO}(T_{w,i} - T_f) \tag{2.25}$$

$$q''_{ONB} = [\frac{\Delta T_{sat}(1082P^{1.156})^n}{0.556}]^{1/n} \tag{2.26}$$

where P is in bars and ΔT_{sat} is in K. The factor n can be calculated as follows.

$$n = 0.463P^{0.0234} \tag{2.27}$$

where P is in bars.

2.4 Uncertainty Analysis

The uncertainties of the measured values are given in Table 2.1 and 2.2. They were provided by the manufacturer's specification sheet, whereas the uncertainties on friction factors and heat transfer coefficients were obtained using the propagation of uncertainty method developed by Kline and McClintock [63].

This method is based on careful specifications of the uncertainties in various primary experimental measurements. Let w_R be the uncertainty in the result and w_1, $w_{2,\ldots}$, w_n be the uncertainties in the independent variables. If the uncertainties in the independent variables are all given with the same ratios, then the uncertainty in the result having these ratios is given as:

$$w_R = [(\frac{\partial R}{\partial x_1}w_1)^2 + (\frac{\partial R}{\partial x_2}w_2)^2 + \ldots + (\frac{\partial R}{\partial x_n}w_n)^2]^{1/2} \tag{2.28}$$

Here R is the result value, where x_1, $x_2,\ldots,x_n$ are independent variable's values.

Moreover, Mean Absolute Error (MAE) is a quantity used to measure how close predictions are to the eventual outcomes. The MAE is given by:

$$MAE = \frac{1}{n}\sum_{i=1}^{n} | f_i - y_i | \quad (2.29)$$

where f_i is the prediction, y_i is the true value, and N is the number of experimental data.

Table 2.1: Uncertainties in single-phase experimental parameters

Uncertainity	**Error**
Flow Rate, Q (for each reading)	$\pm$ 1.0 %
Voltage supplied by power source, V	$\pm$ 0.1 %
Current supplied by power source, I	$\pm$ 0.1 %
Temperature, T	$\pm$ 0.1℃
Electrical power, P	$\pm$ 0.15 %
Pressure drop, ΔP	$\pm$ 0.25 %
Mass flux, G	$\pm$ 2.7 %
Friction factor, f	$\pm$ 7 %
Hydraulic diameter, d_h	$\pm$ 2 μm
Heat transfer coefficient, h_{sp}	$\pm$ 10.7 %
Nusselt number, Nu	$\pm$ 11 %

Table 2.2: Uncertainties in two-phase experimental parameters

Uncertainity	**Error**
Flow Rate, Q (for each reading)	$\pm$ 1.0 %
Voltage supplied by power source, V	$\pm$ 0.1 %
Current supplied by power source, I	$\pm$ 0.1 %
Temperature, T	$\pm$ 0.1℃
Electrical power, P	$\pm$ 0.15 %
Pressure drop, ΔP	$\pm$ 0.25 %
Mass flux, G	$\pm$ 2.7 %
Friction factor, f	$\pm$ 7 %
Hydraulic diameter, d_h	$\pm$ 2 μm
Heat transfer coefficient, htp	$\pm$ 11.9 %

CHAPTER 3

RESULTS AND DISCUSSIONS

3.1 Single-Phase Flow Part

In this section, single-phase fluid flow experimental results will be included. Friction factor, local single-phase heat transfer coefficients, and ratio of theoretical Nusselt number to experimental Nusselt number results will be displayed and discussed.

3.1.1 Friction Factor Results

Initially, adiabatic tests were carried out and satisfactorily compared to the existing conventional friction factor correlation recommended for fully developed laminar flows in tubes (f=64/Re). As shown in Fig. 3.1, experimental data could be predicted fairly well by the existing correlation for laminar flow conditions with a Mean Absolute Error (MAE) of 21%. This result is in agreement with the previous comparison studies on friction factors [28, 30, 37, 38], which also reported that friction factors in microchannels in fully developed flow could be predicted by the existing theory developed for conventional channels. Moreover, this fair prediction also implies that hydrodynamically developed flow conditions are present in the current study. The hydrodynamic developing length for Re=1087 is 1.5cm for 254 micron tube, and 4.01 cm for 685 micron tube, which is significantly lower than the entire channels length of 14.88 cm and 15.24 cm, respectively. Thus, hydrodynamic fully developed flow conditions are not surprising in this study.

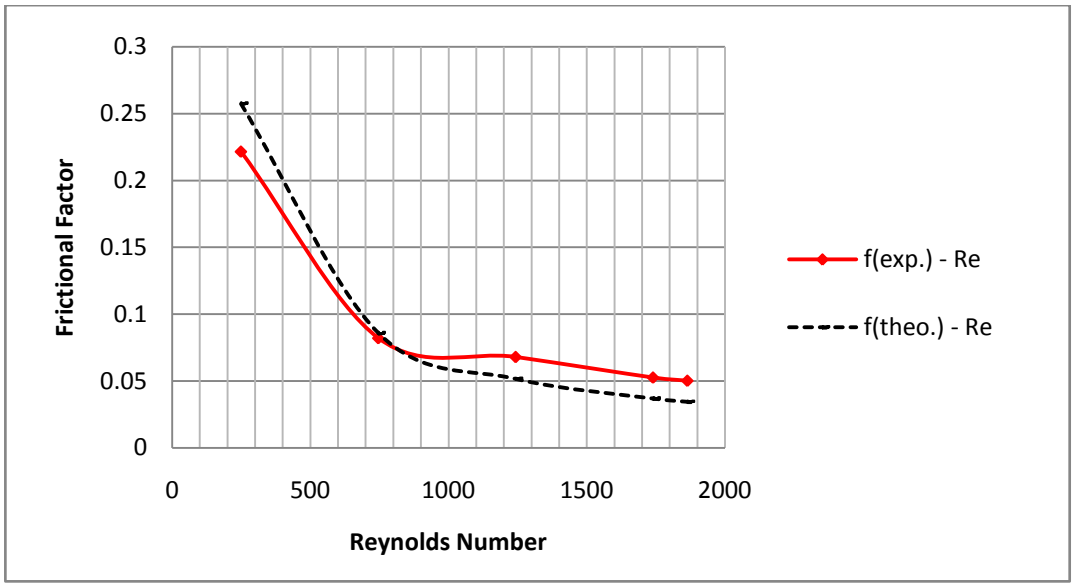

Figure 3.1: Friction Factors – Reynolds Number Profile

In addition to these findings, diabatic tests have been also carried out for the same microchannel configuration to observe laminar-turbulent transition. The transition from laminar flow to turbulent flow for the same configuration is detected with the shift in the trend of f vs Re curve in Fig. 3.2 and Fig. 3.3 for 254 micron tube and 685 micron tube respectively. It can be seen that the transition of Reynolds number occurs between 2500-3000 due to the change in the trend, which could not be characterized as an early transition. This transition could be also regarded as a sudden transition [28]. Lorenzini et al. [28] indicated that sudden laminar to turbulent transition seems to become the prevailing mode when the critical Reynolds number is greater than 2300 regardless the surface of the microtubes (i.e. either smooth or rough). As a result, laminar to turbulent transition in this study could be also regarded as a sudden transition.

For the turbulent portion of the experimental data, Colebrook correlation was used and compared to experimental data. A relative roughness was taken as 0.004 in the light of measured peak to peak roughness and microtube dimensions. Accordingly, the MAE in friction factor is calculated as 19.3% and 10.3% for 254 micron tube and 685 micron tube respectively, which suggests that friction factor correlations for turbulent flows could also fairly predict turbulent flow data in micro scale. These results are in good agreement with the existing literature about micro scale fluid flow [28, 64].

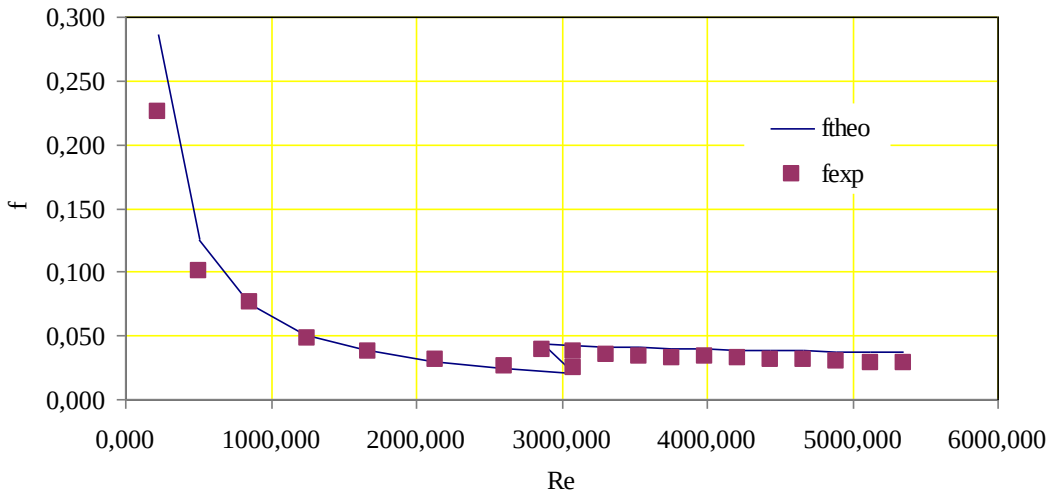

Figure 3.2: Friction Factors – Reynolds Number Profile for 254 micron tube

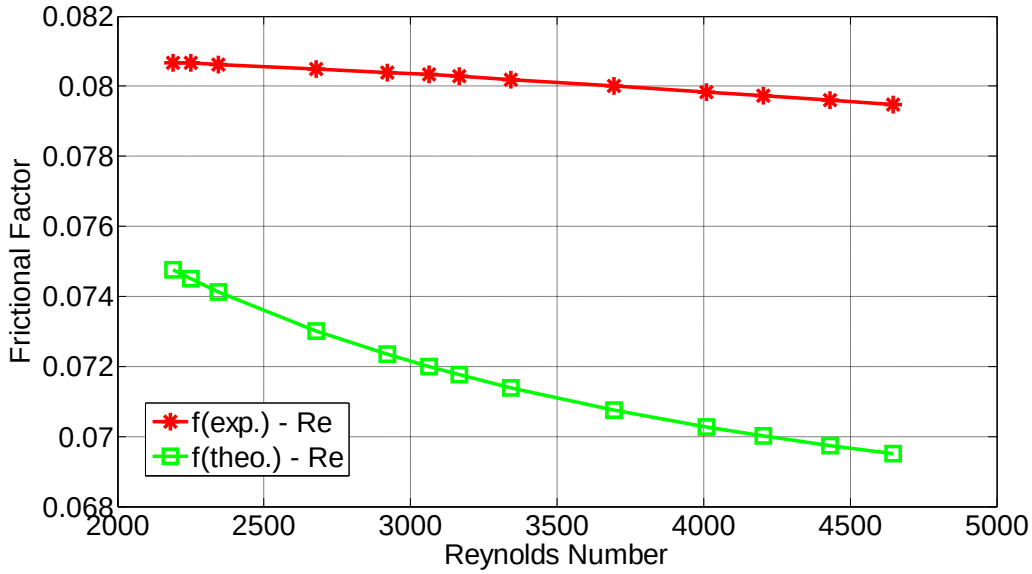

Figure 3.3: Friction Factors – Reynolds Number Profile for 685 micron tube

3.1.2 Heat Transfer Results

In Figs. 3.4-3.9, inner wall temperatures were presented for each thermocouple location at different mass fluxes for both microtubes. Inner wall temperatures increase with heat flux as expected. Moreover in Figs. 3.10-3.15 local single phase heat transfer coefficients were presented for each thermocouple location at different mass fluxes. As

seen from these figures, single phase heat transfer coefficients increase as mass flux increases. In addition, we can observe that the increase in mass flux results in lower channel surface temperatures at constant heat fluxes. The increasing trend in local heat transfer coefficients with mass flux is due to developing flow conditions and also provides high motivation for working at high mass fluxes, so that high heat transfer coefficients could be reached even in single phase flow (>40000 W/m^{2}C) as seen in Figs. 3.10-3.15. Heat flux values in these figures are much greater than in literature [37] due to the high mass fluxes and thermally developing flow conditions in this thesis.

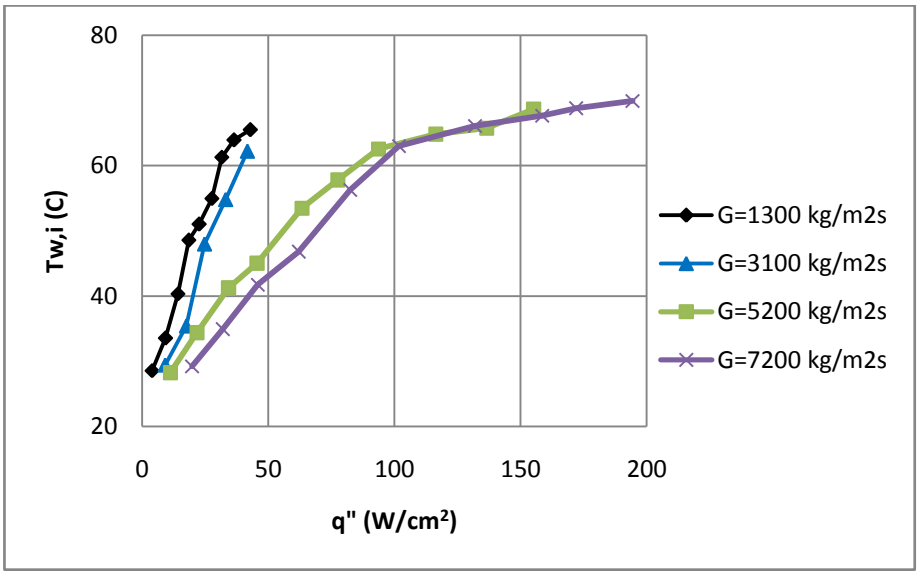

Figure 3.4: Inner wall temperatures – heat flux profile for thermocouple 1 in 254 micron tube

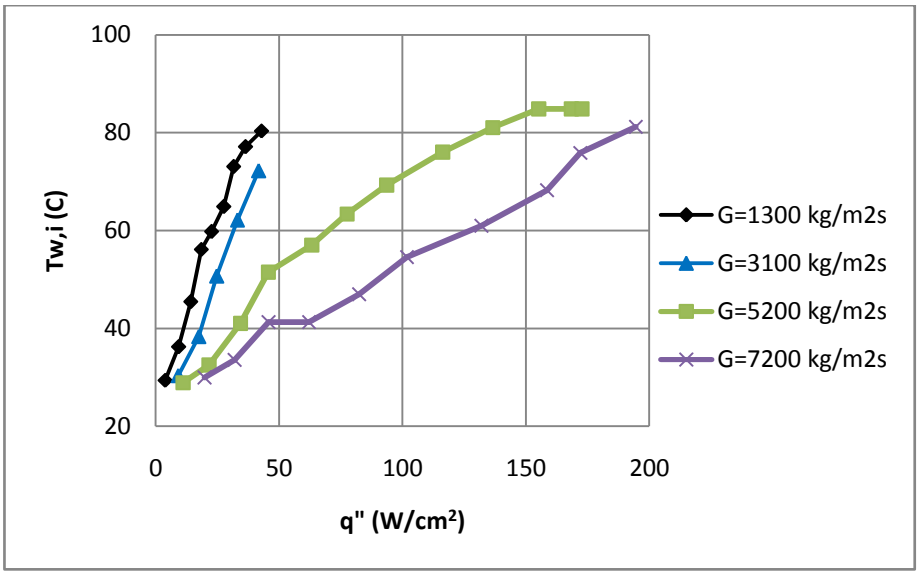

Figure 3.5: Inner wall temperatures – heat flux profile for thermocouple 2 in 254 micron tube

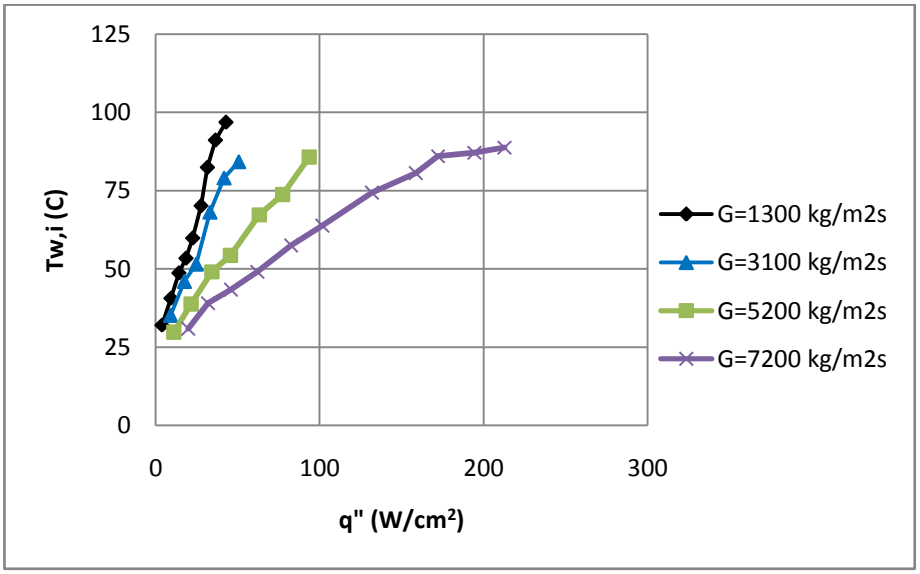

Figure 3.6: Inner wall temperatures – heat flux profile for thermocouple 3 in 254 micron tube

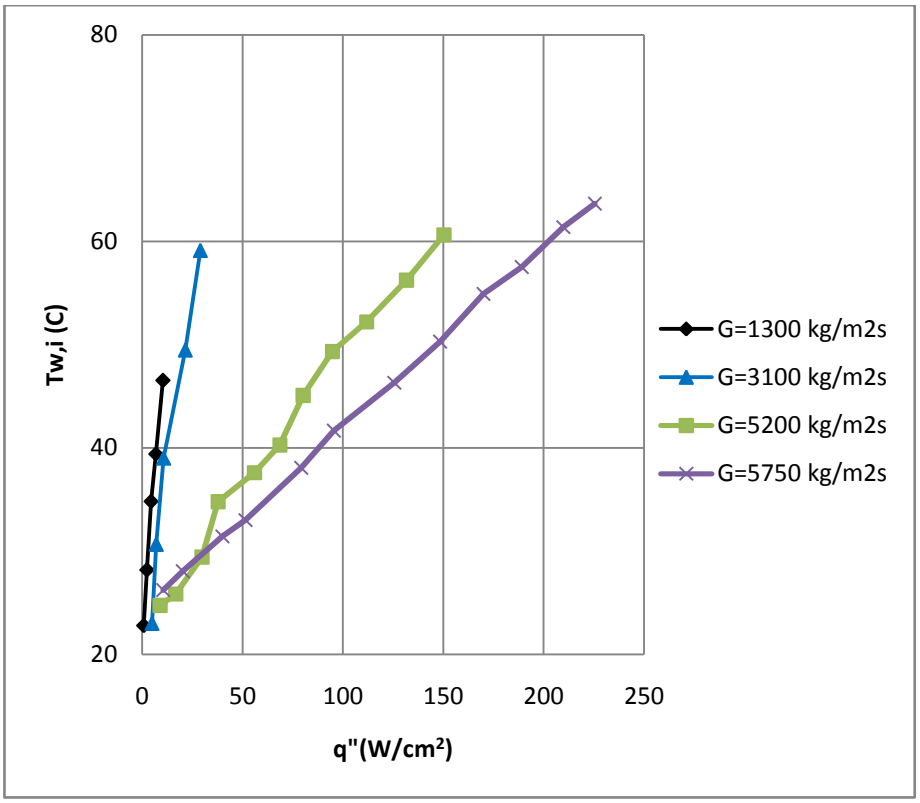

Figure 3.7: Inner wall temperatures – heat flux profile for thermocouple 1 in 685 micron tube

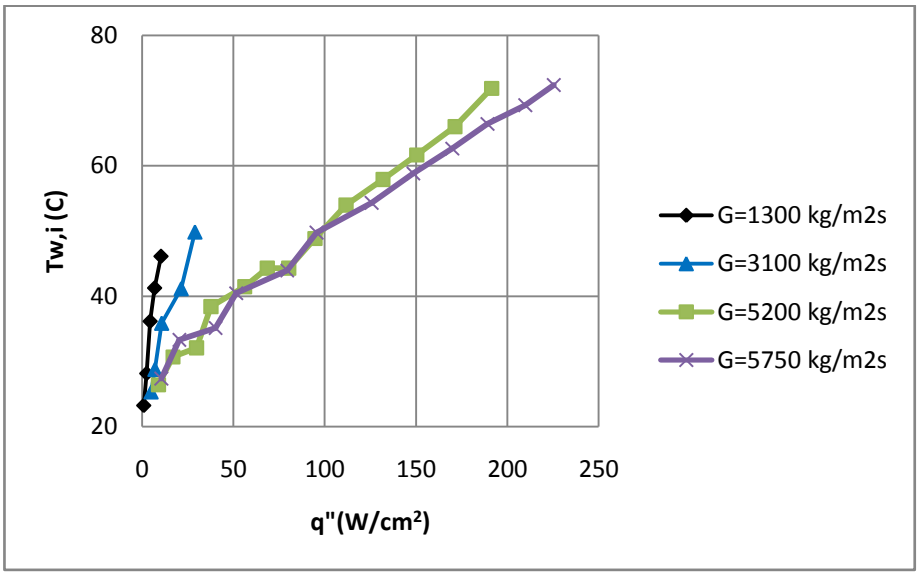

Figure 3.8: Inner wall temperatures – heat flux profile for thermocouple 2 in 685 micron tube

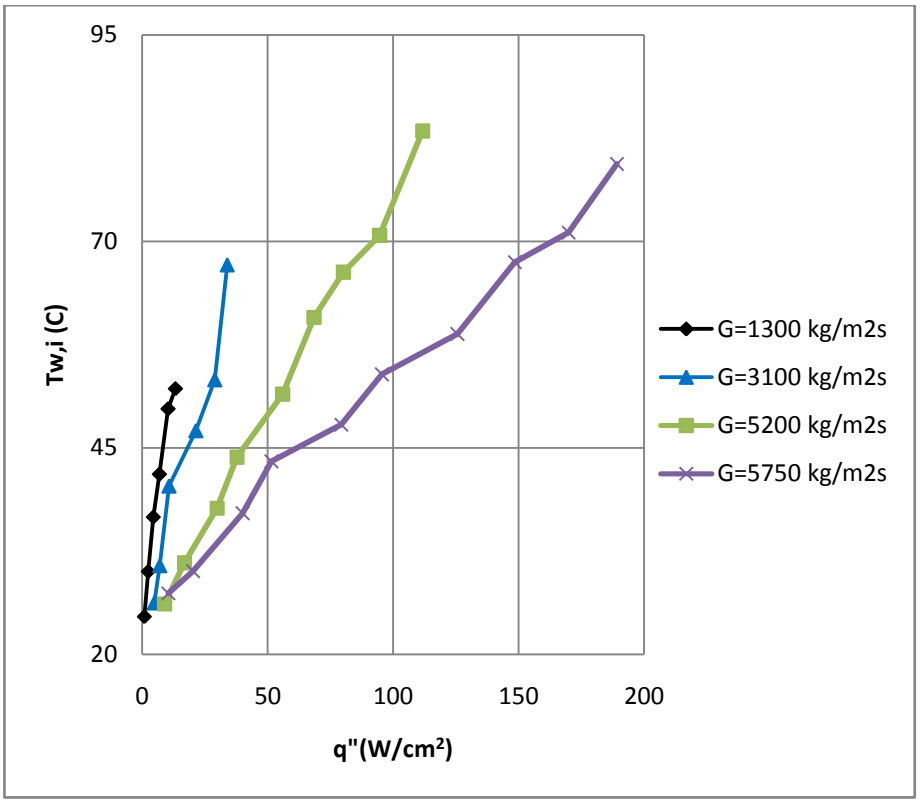

Figure 3.9: Inner wall temperatures – heat flux profile for thermocouple 3 in 685 micron tube

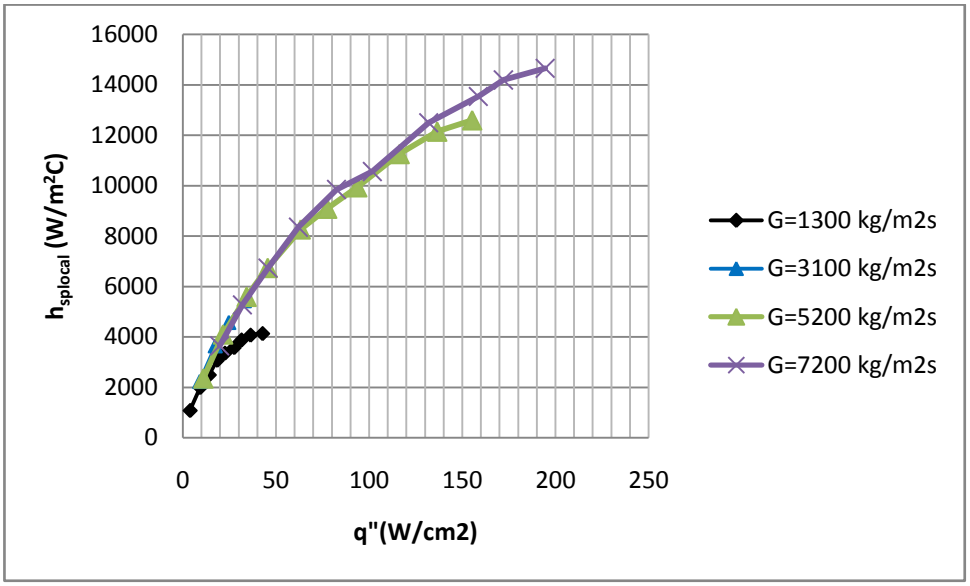

Figure 3.10: Local single-phase heat transfer coefficients – heat flux profile for thermocouple 1 in 254 micron tube

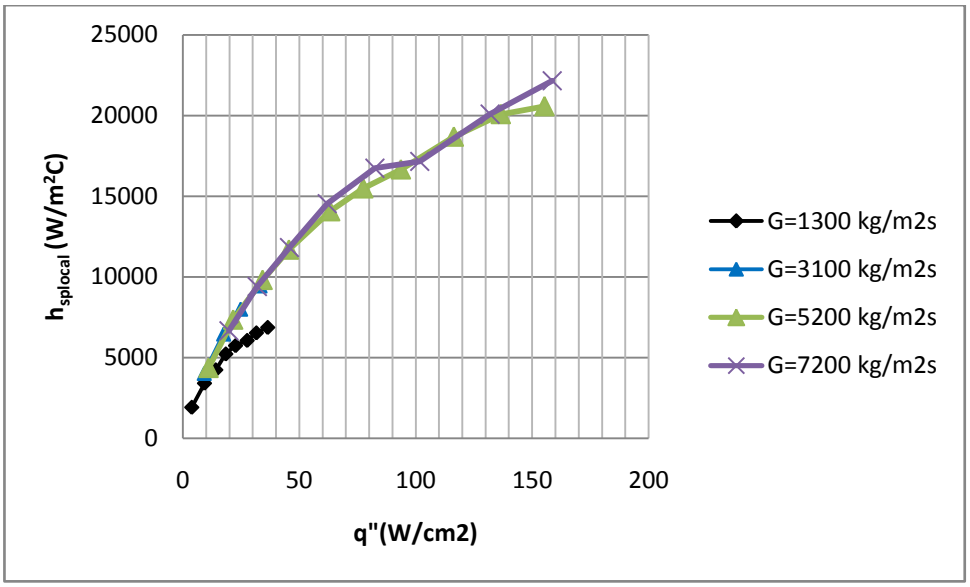

Figure 3.11: Local single-phase heat transfer coefficients – heat flux profile for thermocouple 2 in 254 micron tube

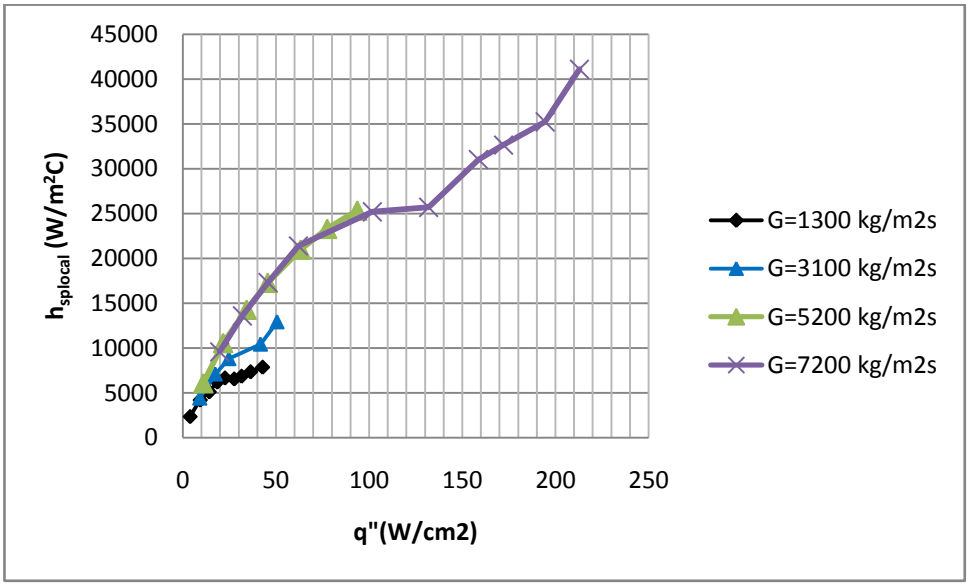

Figure 3.12: Local single-phase heat transfer coefficients – heat flux profile for thermocouple 3 in 254 micron tube

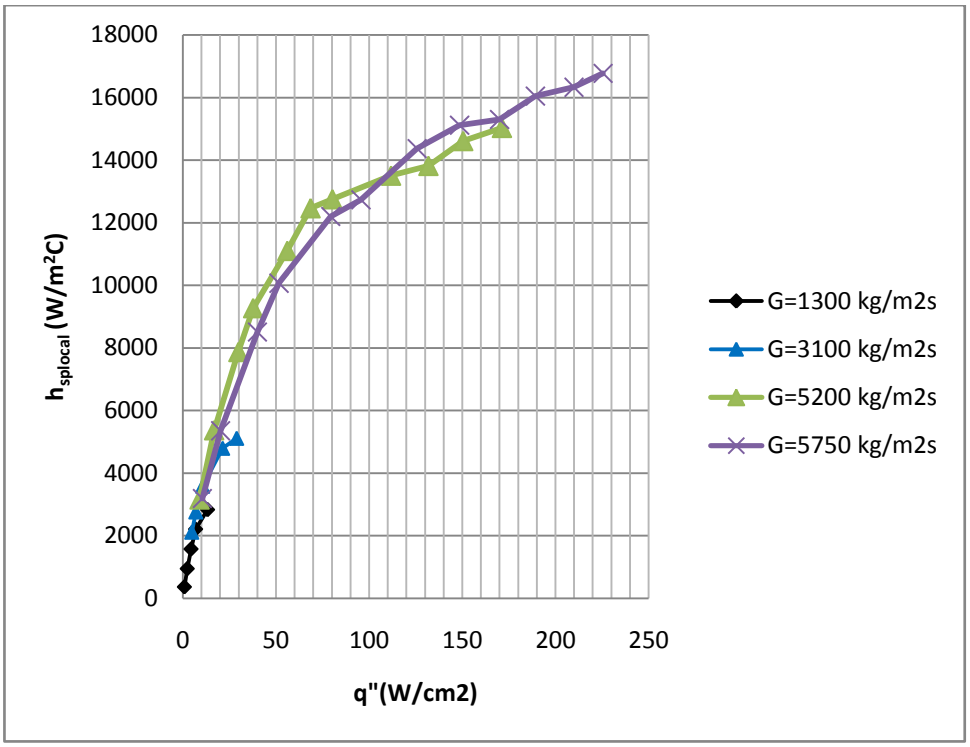

Figure 3.13: Local single-phase heat transfer coefficients – heat flux profile for thermocouple 1 in 685 micron tube

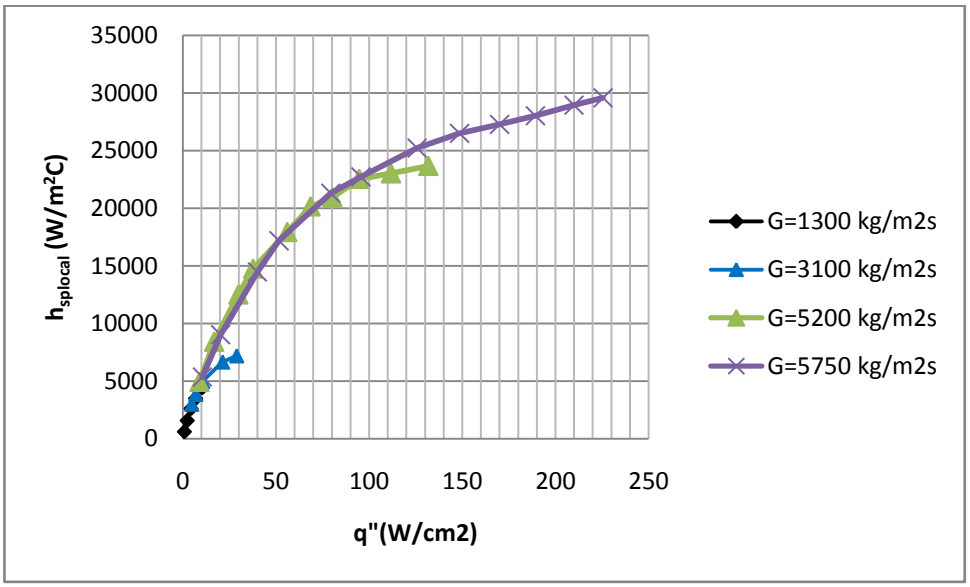

Figure 3.14: Local single-phase heat transfer coefficients – heat flux profile for thermocouple 2 in 685 micron tube

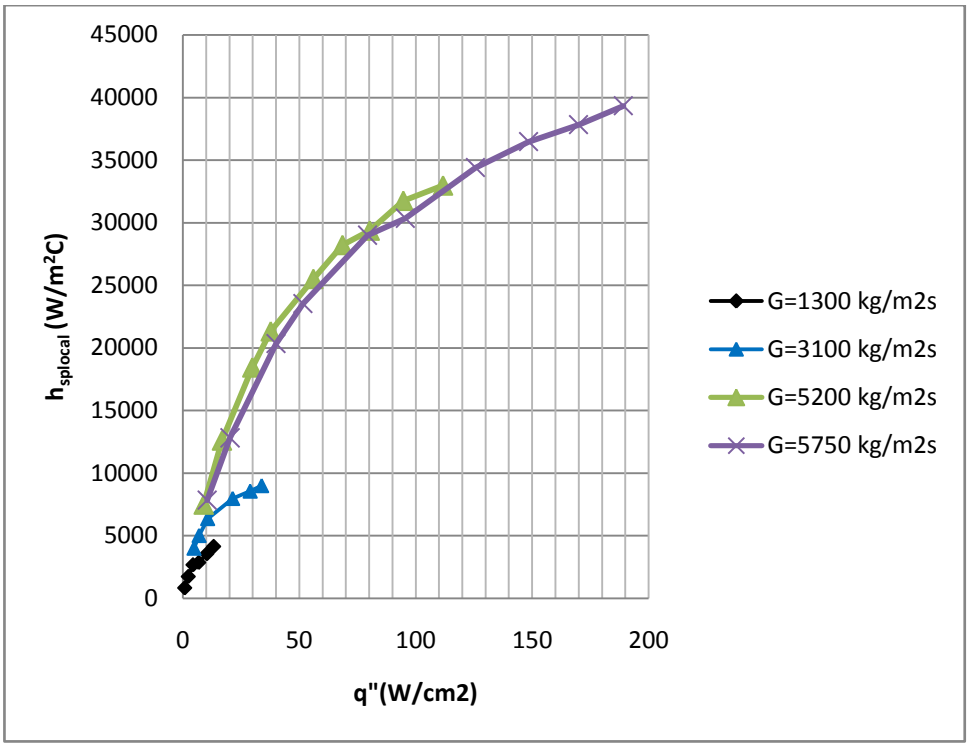

Figure 3.15: Local single-phase heat transfer coefficients – heat flux profile for thermocouple 3 in 685 micron tube

The comparison between theoretical and experimental Nusselt numbers is demonstrated in Figs. 3.16-3.21 for each thermocouple location. $Nu_{x,H1}$ is the theoretical thermally developing Nusselt number depending on the location x_{th}, while Nu is the corresponding experimental Nusselt number. For laminar flow conditions, Eq. 2.10 was used for calculating $Nu_{x,H1}$, while under turbulent conditions Eq. 2.13 was used for calculating $Nu_{x,H1}$. As seen from these figures almost, every data point could be predicted within $\pm$ 50 % by the existing correlations. The resulting total MAE is 24%. These results show that experimental Nusselt numbers could be reasonably predicted by theoretical Nusselt numbers for developing flow conditions. This also strengthens the claim in the literature [62] that conventional correlations could be applicable to single-phase flows in micro scale. However, they could not follow the trend in experimental data very well.

In addition, the success of thermally developing flow correlations also emphasize on developing effects on heat transfer. In the current study the thermally developing lengths of 254 micron tube for G=1300, 3100, 5200 and 7200 are 3.5cm, 7.1cm,

11.22cm and 15.74cm respectively, while the thermally developing lengths of 685 micron tube for G=1300, 3100, 5200 and 5750 are 2.5cm, 5.8cm, 9.62cm and 10.59cm, respectively. Most of these values are greater than the heated length. Thus, developing effects are prevalent along the entire heated length leading to high heat transfer coefficients and Nusselt numbers when compared to thermally fully developed flows.

For thermocouple locations 1 and 2 the experimental results are closer to the theory (MAE=19.2, 20.8, respectively) compared to thermocouple location 3 (MAE=23.6). It can be clearly seen that while Re increases experimental results better agree with the theoretical results for thermocouple locations 1 and 2. This trend is present because thermocouples 1 and 2 are located closer to the micro tube inlet, where developing effects are more dominant.

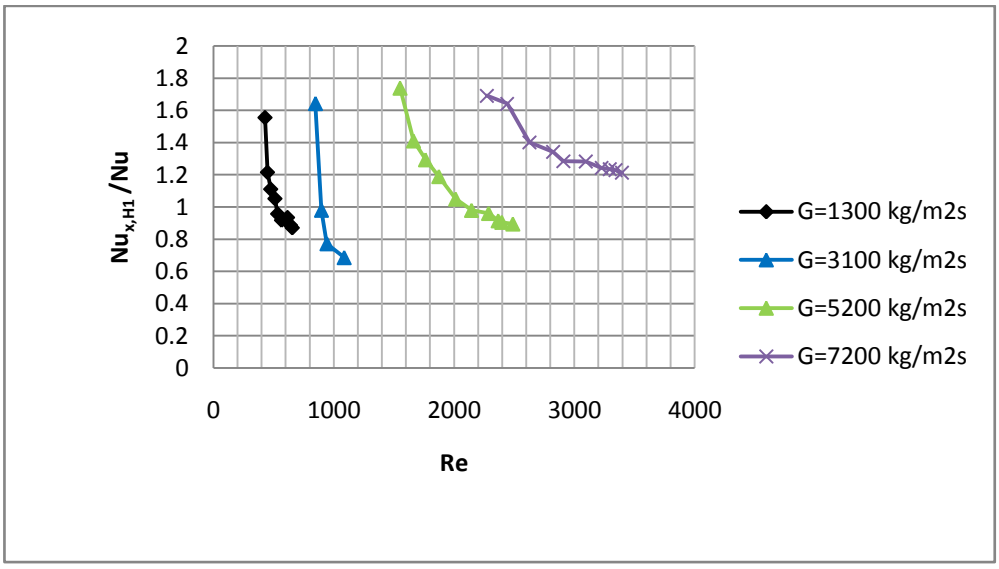

Figure 3.16: Ratio of theoretical Nusselt number to experimental Nusselt number for thermocouple 1 in 254 micron tube

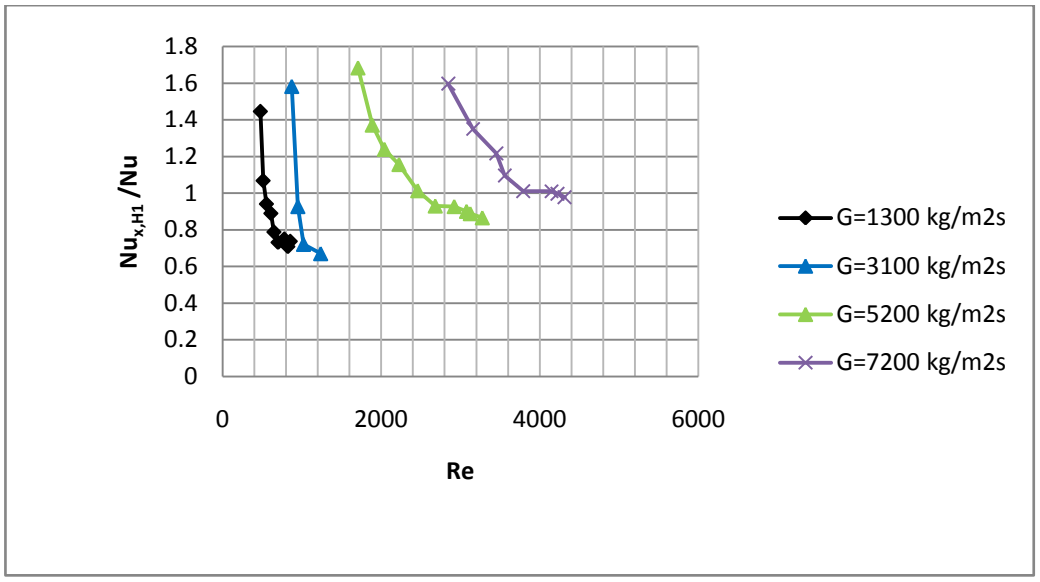

Figure 3.17: Ratio of theoretical Nusselt number to experimental Nusselt number for thermocouple 2 in 254 micron tube

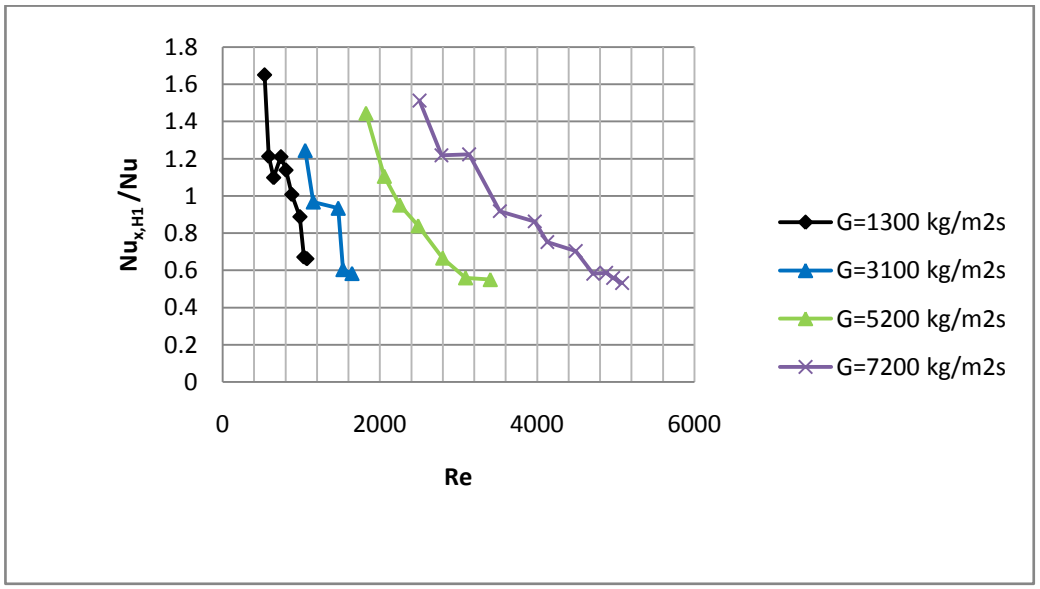

Figure 3.18: Ratio of theoretical Nusselt number to experimental Nusselt number for thermocouple 3 in 254 micron tube

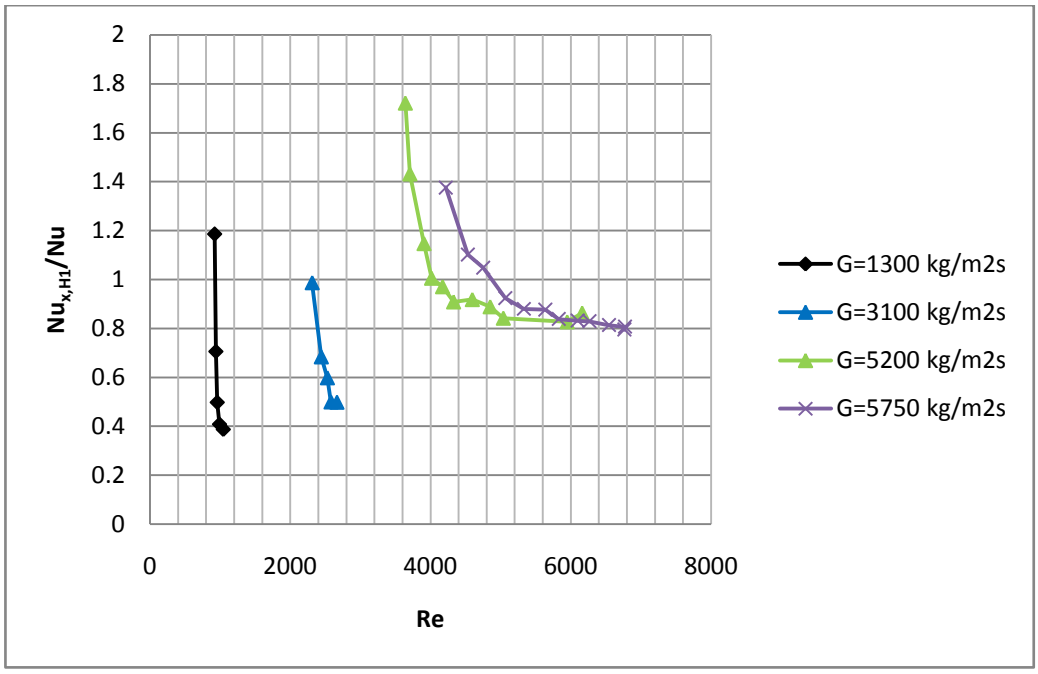

Figure 3.19: Ratio of theoretical Nusselt number to experimental Nusselt number for thermocouple 1 in 685 micron tube

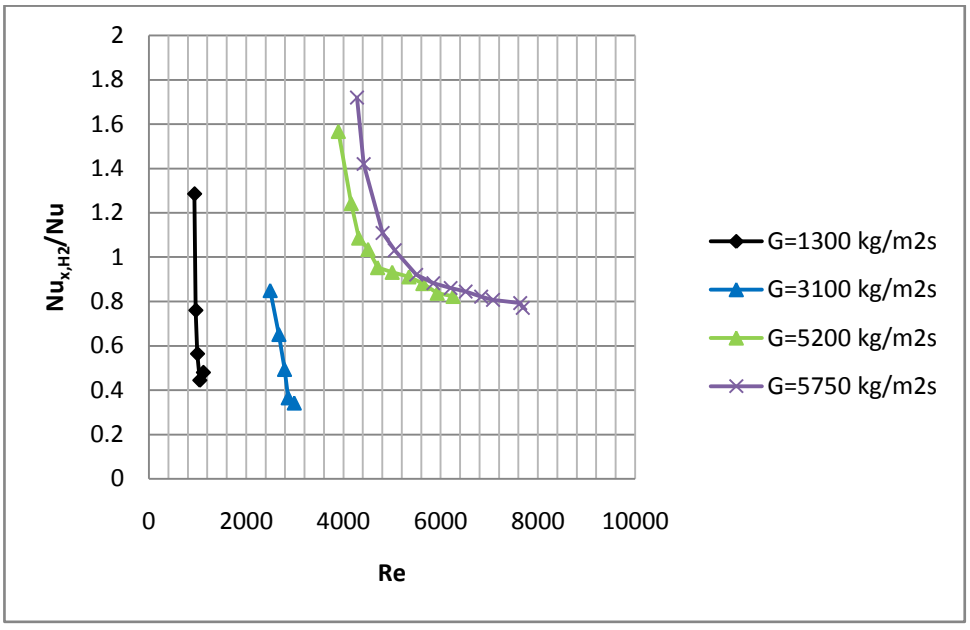

Figure 3.20: Ratio of theoretical Nusselt number to experimental Nusselt number for thermocouple 2 in 685 micron tube

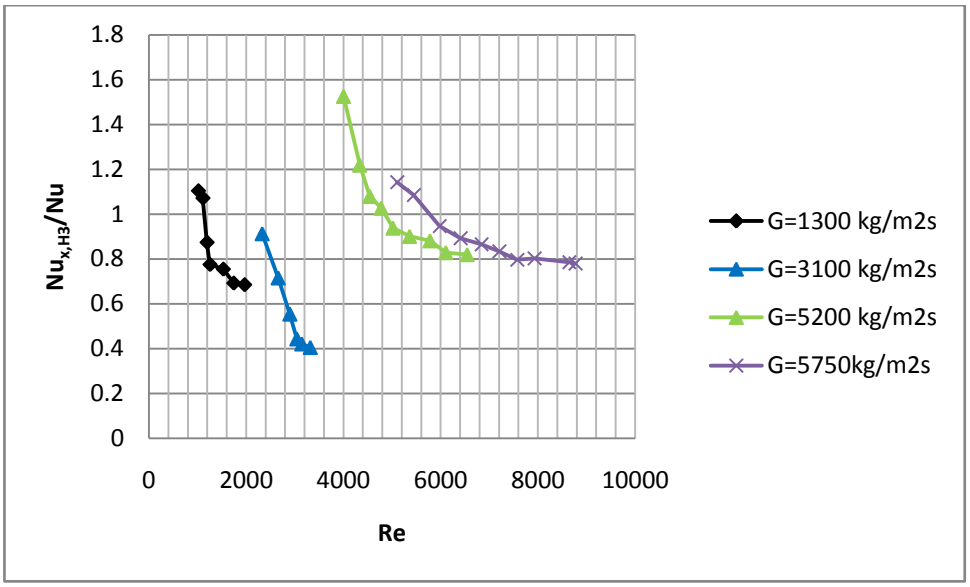

Figure 3.21: Ratio of theoretical Nusselt number to experimental Nusselt number for thermocouple 3 in 685 micron tube

3.2 Boiling Heat Transfer Part

Wall superheats are displayed with heat flux for thermocouples 2 and 3 in Figs. 3.22 - 3.24. Since the saturation temperature for the thermocouple location 2 is greater than the saturation temperature of the thermocouple location 3 and the wall temperature did not increase significantly along the microtube, fewer data points are present for thermocouple 2. It could be clearly seen that at a fixed wall superheat, the heat flux increases with mass velocity implying better heat removal rates at higher mass velocities.

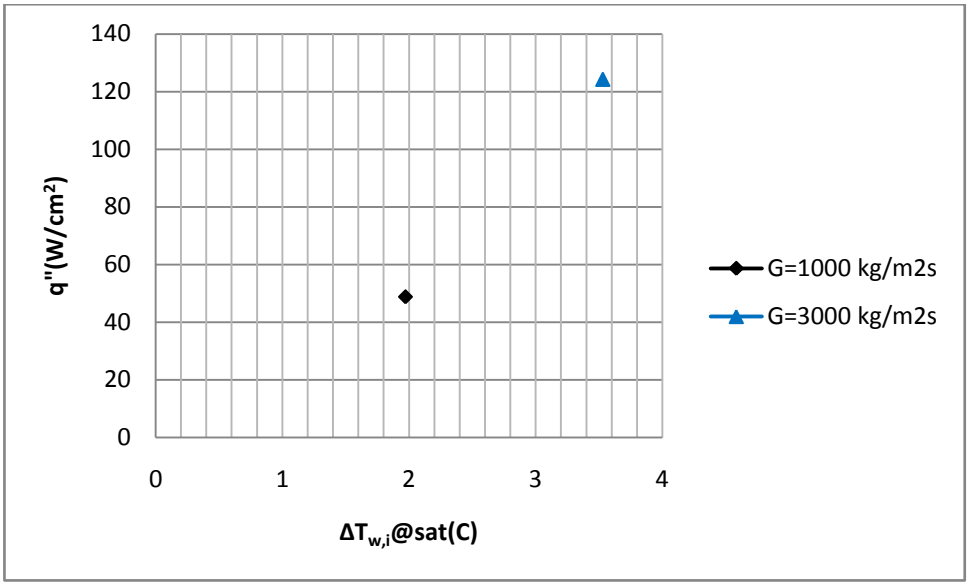

Figure 3.22: Heat Flux- Local $\Delta T_{w,i}$ at saturation for thermocouple 2 location (x_{th2}) at different mass fluxes for 254 micron tube

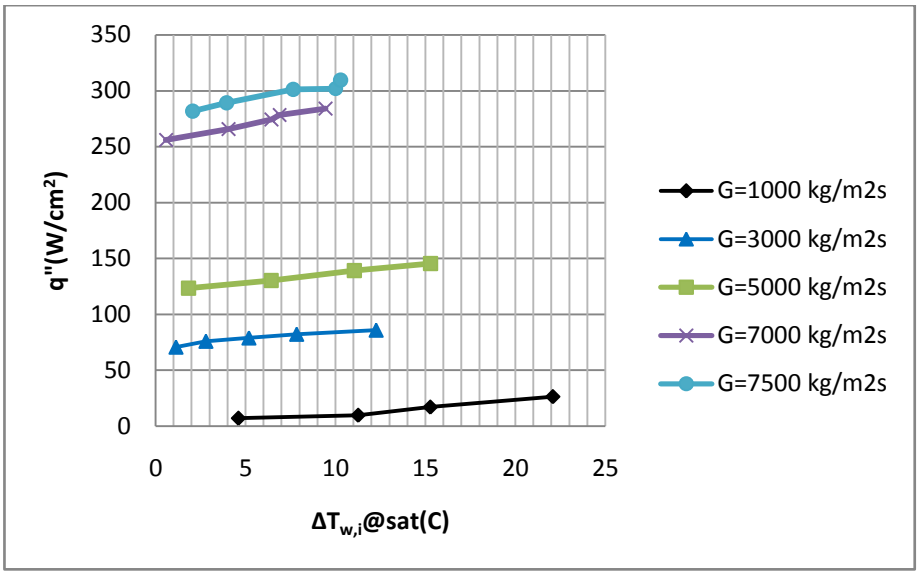

Figure 3.23: Heat Flux- Local $\Delta T_{w,i}$ at saturation for thermocouple 3 location (x_{th3}) at different mass fluxes for 254 micron tube

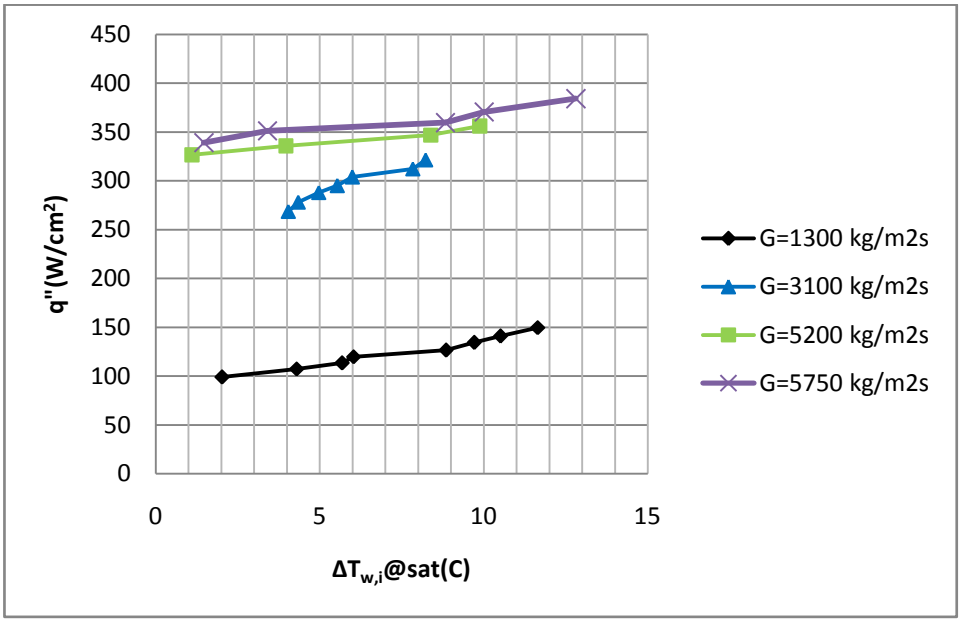

Figure 3.24: Heat Flux- Local $\Delta T_{w,i}$ at saturation for thermocouple 3 location (x_{th3}) at different mass fluxes for 685 micron tube

During the tests it has been assured that subcooled conditions are present.Higher heat transfer coefficients are obtained for higher mass velocity at the resulting heat fluxes. A strong dependence of heat transfer coefficients on mass velocity is apparent in Figs. 3.25 to 3.27. Rohsenow [65] suggested that heat transfer coefficient is a sum of

single-phase and nucleate boiling components for subcooled boiling conditions. Single-phase component is mass velocity dependent, whereas the nucleate boiling component is highly wall superheat dependent and mass velocity independent. The strong mass velocity dependence in this study suggests that single-phase flow effects are still present under the working conditions of this study.

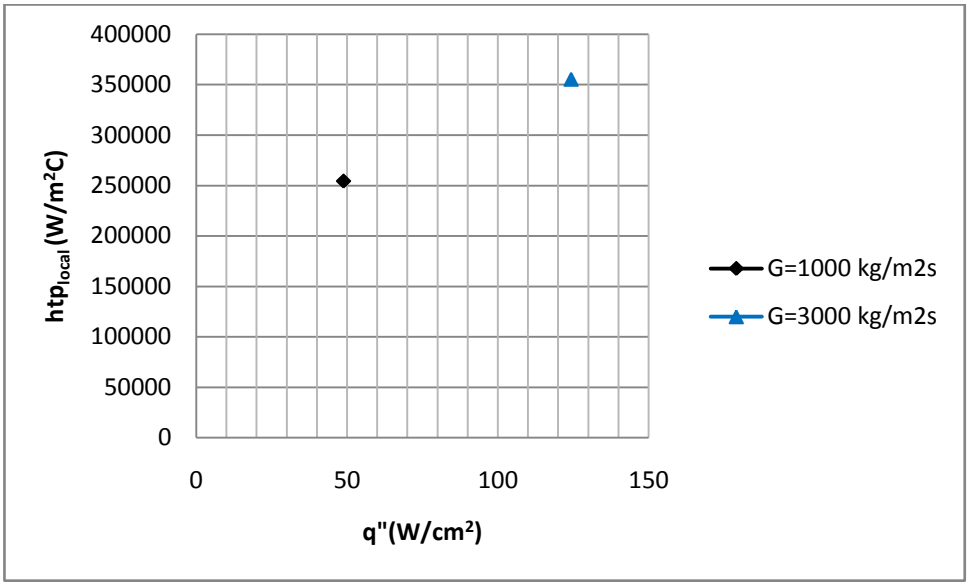

Figure 3.25: Local two-phase heat transfer coefficient – Heat flux for thermocouple 2 locations (x_{th2}) at different mass fluxes for 254 micron tube

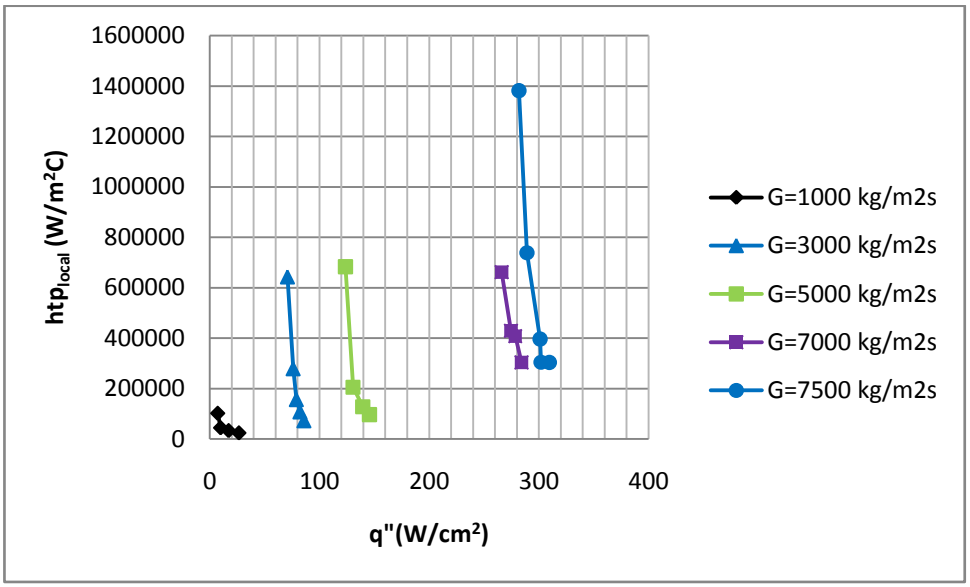

Figure 3.26: Local two-phase heat transfer coefficient – Heat flux for thermocouple 3 locations (x_{th3}) at different mass fluxes for 254 micron tube

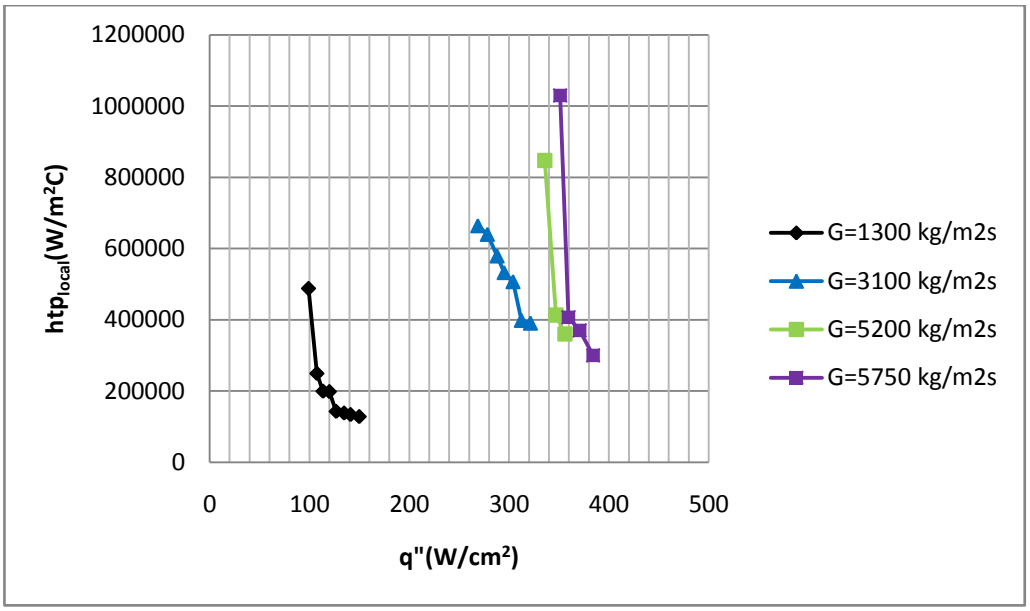

Figure 3.27: Local two-phase heat transfer coefficient – Heat flux for thermocouple 3 locations (x_{th3}) at different mass fluxes for 685 micron tube

Figures 3.28 to 3.30 show the dependence of heat transfer coefficient on the quality. Heat transfer coefficients show a similar trend with quality as heat flux. With increasing quality, heat transfer coefficients have a decreasing trend.

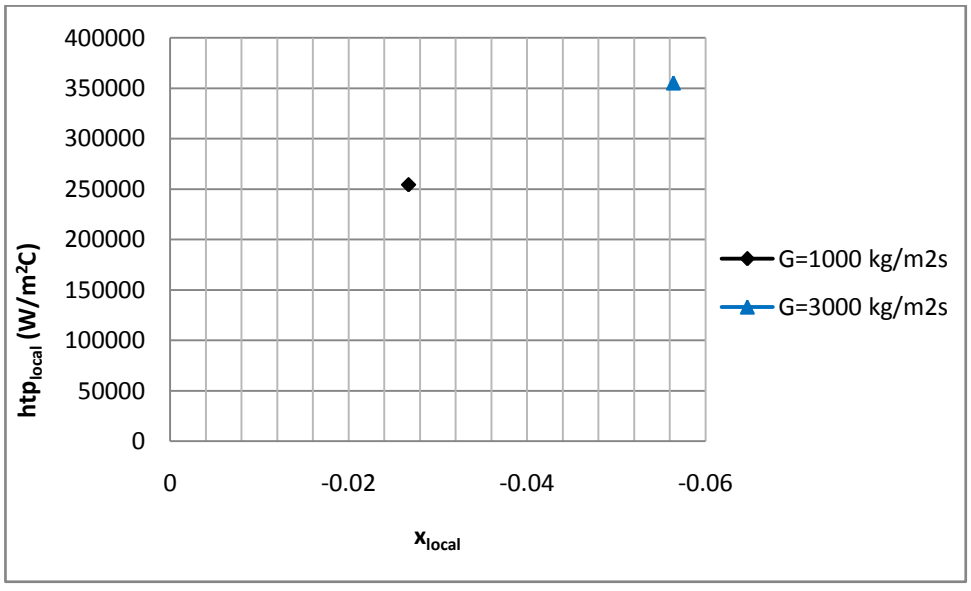

Figure 3.28: Local two-phase heat transfer coefficient – local qualities for thermocouple 2 location (x_{th2}) at different mass fluxes

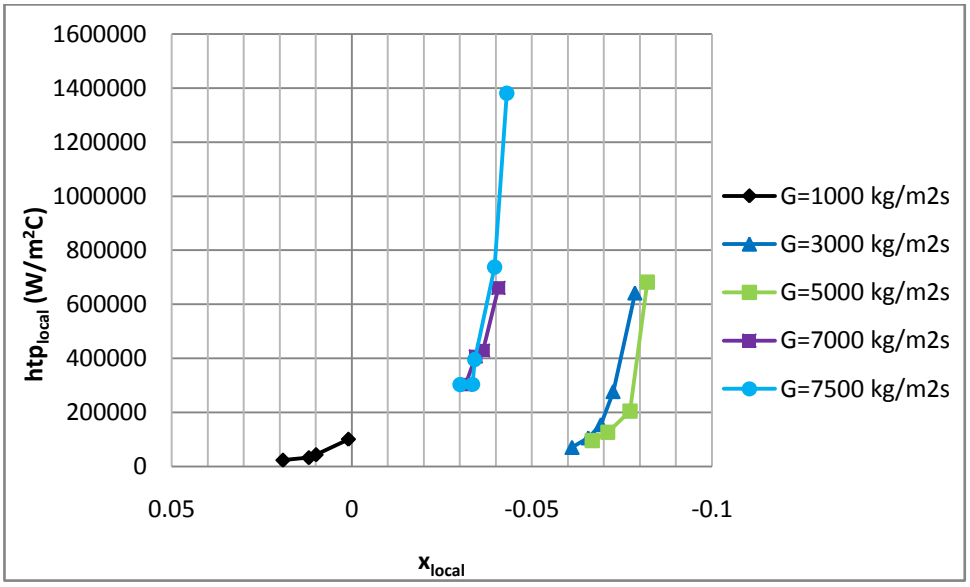

Figure 3.29: Local two-phase heat transfer coefficient – local qualities for thermocouple 3 location (x_{th3}) at different mass fluxes for 254 micron tube

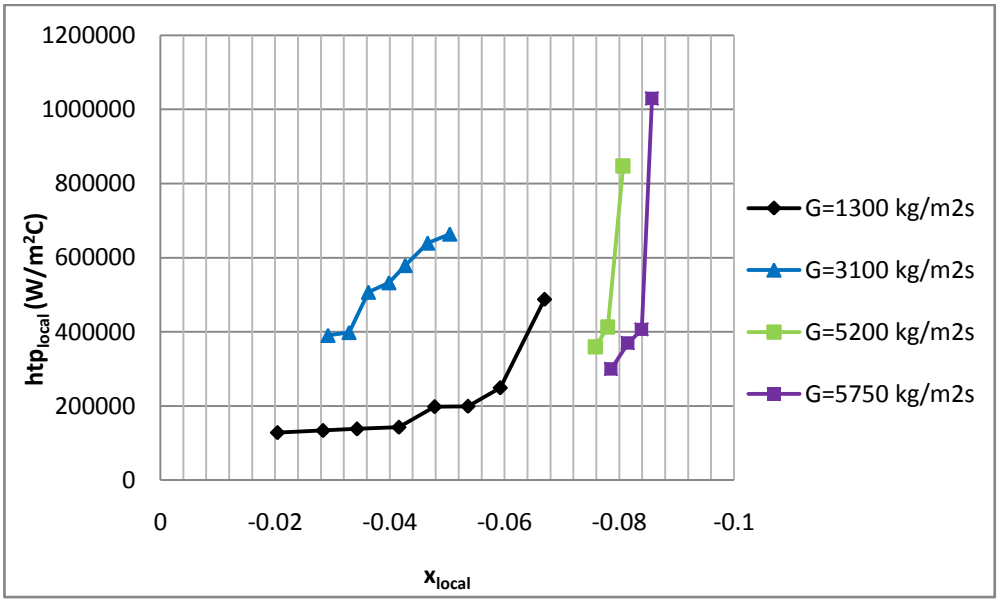

Figure 3.30: Local two-phase heat transfer coefficient – local qualities for thermocouple 3 location (x_{th3}) at different mass fluxes for 685 micron tube

In Fig. 3.31, 3.32 and Tables 3.1 to 3.4 experimental heat fluxes were compared with partial boiling correlations and fully developed subcooled boiling correlations. It is seen that at low ΔT_{sat} values, there is only small deviation between the experimental data and partial boiling correlations (MAE % 0.5 to % 20), while subcooled fully developed correlations predictions could fairly predict experimental results well at only high ΔT_{sat} values. Kandlikar et al. [51] proposed that in order to use fully developed subcooled flow boiling correlations, ΔT_{sat} values should be higher than ~30℃. In this study, the maximum ΔT_{sat} was 21 ℃. In addition to this, at high mass fluxes there is a better agreement between correlations and experimental data, because for lower mass fluxes the corresponding Reynolds numbers are in the transition regime where the prediction of single-phase heat transfer coefficients are not clearly determined.

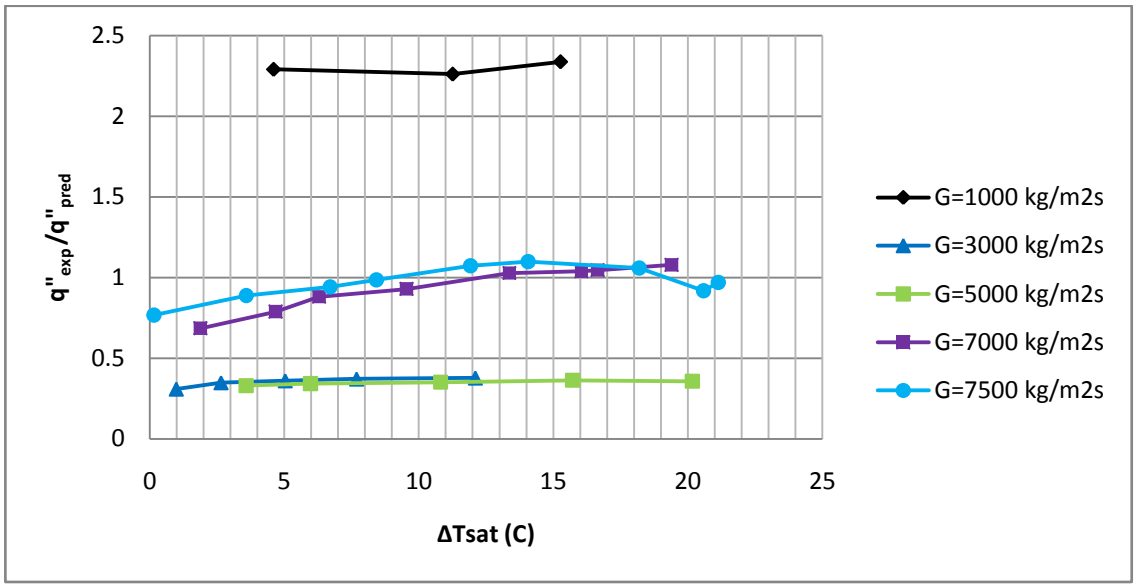

Figure 3.31: $q''_{experimental}$ /$q''_{predicted}$ - $\Delta T_{saturation}$ at different mass fluxes for 254 micron tube

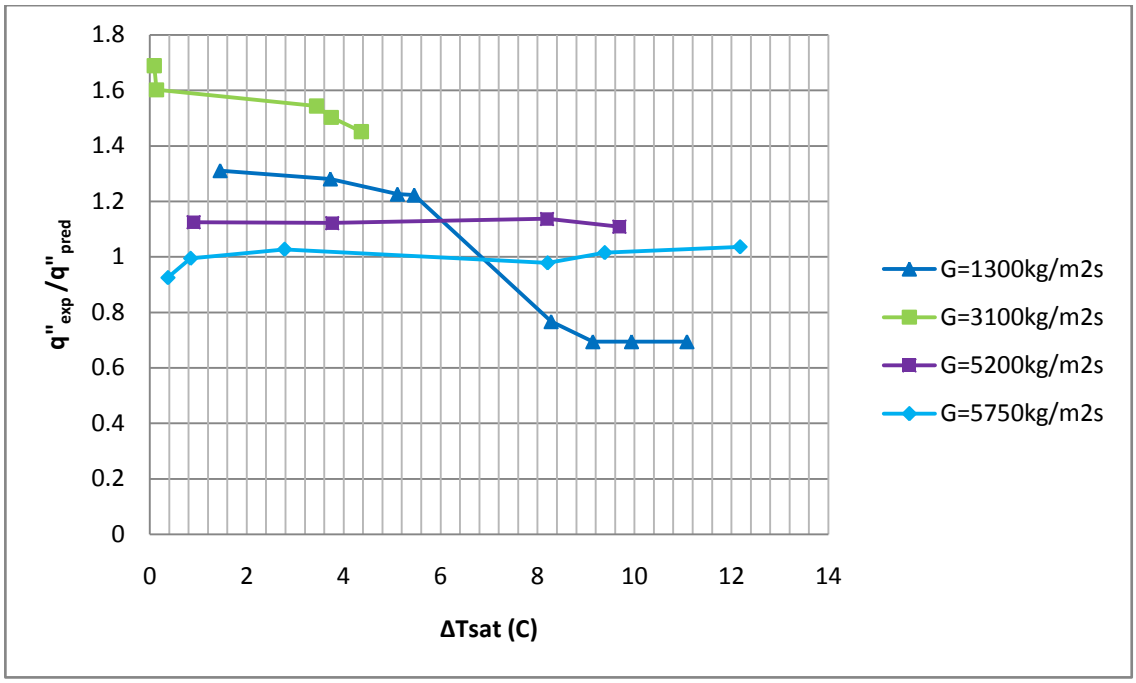

Figure 3.32: $q''_{experimental}/q''_{predicted}$ - $\Delta T_{saturation}$ at different mass fluxes for 685 micron tube

Table 3.1 : MAE Comparison between fully developed subcooled boiling and partial boiling correlations with experimental data for 254 micron tube at G=7000 kg/m^2s

$q''_{exp.}$ (W/m^2)	q''_{fully} (W/m^2)	$q''_{partial}$ (W/m^2)	ΔT_{sat} (C)
2236011	2836	2.84E+06	1.87
2344592	42426	2.66E+06	4.668
2411027	101167	2.59E+06	6.283
2546604	338368	2.48E+06	9.536
2644457	893300	2.55E+06	13.36
2729552	1502000	2.61E+06	16.04
2771205	1658000	2.57E+06	16.64
2827554	1456000	2.88E+06	19.39

Table 3.2 : MAE Comparison between fully developed subcooled boiling and partial boiling correlations with experimental data for 254 micron tube at G=7500 kg/m^2s

$q''_{exp.}$ (W/m^2)	q''_{fully} (W/m^2)	$q''_{partial}$ (W/m^2)	ΔT_{sat} (C)
2412851	1.658	3.15E+06	0.1544
2493864	20008	2.81E+06	3.587
2590809	125954	2.75E+06	6.704
2660605	243976	2.70E+06	8.42
2802889	662367	2.61E+06	11.92
2875264	1061000	2.62E+06	14.06
2994732	2202000	2.83E+06	18.19
3006188	1795000	3.28E+06	20.58
3081557	1938000	3.18E+06	21.13

Table 3.3 : MAE Comparison between fully developed subcooled boiling and partial boiling correlations with experimental data for 685 micron tube at G=5200 kg/m^2s

$q''_{exp.}$ (W/m^2)	q''_{fully} (W/m^2)	$q''_{partial}$ (W/m^2)	ΔT_{sat} (C)
3260345	1.62E+02	2.91E+06	9.04E-01
3353007	1.13E+04	2.98E+06	3.76E+00
3464726	1.12E+05	3.13E+06	8.19E+00
3554510	1.82E+05	3.13E+06	9.69E+00

Table 3.4 : MAE Comparison between fully developed subcooled boiling and partial boiling correlations with experimental data for 685 micron tube at G=5750 kg/m^2s

$q''_{exp.}$ (W/m^2)	q''_{fully} (W/m^2)	$q''_{partial}$ (W/m^2)	ΔT_{sat} (C)
3245974	12.2	3.51E+06	0.3709
3387736	138.8	3.41E+06	0.8389
3507080	4910	3.42E+06	2.778
3589961	120507	3.67E+06	8.207
3700343	177017	3.65E+06	9.387
3835184	374473	3.70E+06	12.18

CHAPTER 4

CONTRIBUTION TO THE SCIENTIFIC KNOWLEDGE

Due to aggressive cooling demands in many areas, microchannel heat sinks are one of the major efficient and conventional systems. This thesis aims to fill the gap in single-phase flow and flow boiling at high mass fluxes in microchannels. Contributions to the scientific knowledge of the single-phase flow part are:

- Significant experimental data were acquired for thermally developing flows in microchannels.
- Single-phase heat transfer study has conducted at high mass fluxes in micro scale and it has proven that, it results in high heat transfer coefficients.

Contributions to the scientific knowledge of the flow boiling part are:

- Significant experimental data were gathered for subcooled boiling in microchannels for the first time.
- The trends in two-phase heat transfer coefficients with mass quality, heat and mass fluxes were revealed.
- It was checked whether existing theory for subcooled boiling in conventional channels is applicable for micro scale.

CONCLUSIONS AND FUTURE WORK

In single-phase flow part of this thesis, experimental tests were carried out in micro tubes of ~254 μm and ~685 μm inner diameter at mass velocities from G=1300 kg/m^{2}s to G= 7200 kg/m^{2}s under thermally developing flow conditions. Higher single phase heat transfer coefficients were obtained with increasing mass fluxes, which is motivating to operate at high mass fluxes and under developing flow conditions.

- Theoretical friction factors and Nusselt numbers were compared to the experimental findings.
- A reasonable agreement was found between experimental results and theoretical predictions recommended for heat transfer in thermally developing flows.
- Moreover, the transition to turbulent flow and friction factors for both laminar and turbulent conditions were in agreement with conventional correlations and existing theory.

In the second part of the study, boiling heat transfer study was conducted at for mass velocities from G=1000 kg/m^{2}s to G=7500 kg/m^{2}s under subcooled boiling conditions. It was found that:

- Heat transfer coefficients increased with mass velocity, whereas they decreased with local quality and heat flux.
- Experimental data were compared with partial boiling correlations and fully developed subcooled boiling correlations. It was observed that partial boiling effects were dominant at low ΔT_{sat} values, while fully developed boiling correlations could fairly predict experimental data at high ΔT_{sat} values

As a future work, it is aimed that operating at higher mass fluxes and reaching to a world record in cooling rates (>30000 W/cm^2).

REFERENCES

[1] Feynman, R.P., "There's Plenty of Room at the Bottom", *Journal of Microelectromechanical Systems,* 1, pp. 60-66, **1992.**

[2] Petersen, K.E., "Silicon as Mechanical Material", *Proceeding of the IEEE*, 70, pp. 420-457, **1982.**

[3] Tuckerman, D.B., and Pease, R.F., "High Performance Heat Sinking for VLSI", *IEEE Electronic Device Letters*, EDL-2, pp. 126-129, **1981.**

[4] Nguyen, N-T., and Wereley, S.T., Fundamentals and applications of microfluidics, *Artech House,* Chapter I, **2006**.

[5] Trebotich, D., Zahn, J. D. and Liepmann, D., "Complex Fluid Dynamics in BioMEMS Devices: Modeling of Microfabricated Microneedles", *Technical Proceedings of the 2002 International Conference on Computational Nanoscienceand Nanotechnology, and Technical Proceedings of the Fifth International Conference on Modeling and Simulation of Microsystems,* April 22-25, San Juan, Puerto Rico, **2002**.

[6] Liepmann, D., "Design and Fabrication of a micro-CPL for Chip-Level Cooling", *Proceedings of 2001 ASME International Mechanical Engineering Congress and Exposition*, November 11-16, 2001, New York, NY, **2001.**

[7] Nuñez, M., Polley, G.T., Reyes, E., and Muñoz A., "Surface Selection and design of plate-fin heat exchangers", *Applied Thermal Engineering,* 19, pp. 917-931, **1999**.

[8] Kandlikar, S.G., and Grande, W.J., "Evaluation of Single Phase Flow in Microchannels for High Heat Flux Chip Cooling - Thermohydraulic Performance Enhancement and Fabrication Technology", *Heat Transfer Engineering,* 25, pp. 5-15, **2004.**

[9] Garimella, S.V., and Singhal, V., "Single-Phase Flow and Heat Transport and Pumping Considerations in Microchannel Heat Sinks", *Heat Transfer Engineering*, 25, pp. 15-25, **2004.**

[10] Mudawar, I., and Lee, J., "Two-phase flow in high-heat-flux micro-channel heat sink for refrigeration cooling applications: Part I—pressure drop characteristics", *International Journal of Heat and Mass Transfer*, 48, pp. 928-940, **2005**.

[11] Qu, W., and Mudawar, I., "Measurement and prediction of pressure drop in two-phase micro-channel heat sinks", *International Journal of Heat and Mass Transfer*, 46, pp. 2737-2753, **2003.**

[12] Kosar, A., Kuo, C.J., and Peles, Y., "Suppression of boiling flow oscillations in parallel microchannels with inlet restrictors", *Journal of Heat Transfer*, 128, pp. 251-260, **2006**.

[13] Kosar, A., Ozdemir, M.R., and Keskinoz, M., Pressure drop across micro-pin heat sinks under unstable boiling conditions, *International Journal of Thermal Sciences*, 49, pp. 1253-1263, **2010.**

[14] Khlebtsov, G.N., and Dykman, L.A., "Optical properties and biomedical applications of plasmonic nanoparticles", *Journal of Quantitative Spectroscopy and Radiative Transfer*, 111, pp. 1-35, **2010.**

[15] Baffou, G., Quidant, R., and Abajo, F.J.G., "Nanoscale Control of Optical Heating in Complex Plasmonic Systems", *ACSNANO*, In Press, **2010.**

[16] DiMatteo, R.S., Greiff, P., Finberg, S.L., Young-Waithe, K., Choy, H.K.H., Masaki, M.M., and Fonstad, C.G., "Enhanced photogeneration of carriers in a semiconductor via coupling across a nonisothermal nanoscale vacuum gap", *Appl. Phys. Lett.*, 79, pp. 1894, **2001.**

[17] Francoeur, M., Menguc, M.P., and R. Vaillon, "Near-field radiative heat transfer enhancement via surface phonon-polaritons coupling in thin films," *Appl. Phys. Lett.*, 93, pp. 043109, **2008.**

[18] Fu, C.J., and Tan, W.C., "Near-field radiative heat transfer between two plane surfaces with one having a dielectric coating", *Journal of Quantitative Spectroscopy and Radiative Transfer*, 110, pp. 1027-1036, **2009.**

[19] Sendur, K., Peng, C., and Challener, W., "Near field radiation from a ridge waveguide transducer in the vicinity of a solid immersion lens", *Phys. Rev. Lett.*, 94, pp. 043901, **2005.**

[20] Francoeur, M., Menguc, M.P., and R. Vaillon, "Near-field radiative heat exchanges between two thin films supporting surface phonon-polaritons," *J. Appl. Phys.*, (in press), **2010.**

[21] http://www.draper.com/idd/images/162140-07.jpg

[22] Tabeling, P., "Introduction to Microfluidics", *Oxford University Press*, Ch.1, **2005.**

[23] Courtesy of Analog Devices Company's data.

[24] http://en.wikipedia.org/wiki/File:Electrical-discharge-machine.jpg

[25] Kandlikar, S.G., "Single-phase liquid flow in minichannels and microchannels", *Heat Transfer and Fluid Flow in Minichannels and Microchannels*, Chapter 3 pp. 87-136, **2006.**

[26] Owhaib, W., and Palm, B., "Experimental investigation of single-phase convective heat transfer in circular microchannels", *Experimental Thermal and Fluid Science*, 28, pp. 105-110, **2004.**

[27] Hrnjak, P., and Tu, X., "Single phase pressure drop in microchannels", *International Journal of Heat and Fluid Flow,* 28, pp. 2-14, **2007.**

[28] Lorenzini, M., Morini G. L., and Salvigni, S., "Laminar, transitional and turbulent friciton factors for gas flows in smooth and rough microtubes", *International Journal of Thermal Sciences*, 49, pp. 248-255, **2010.**

[29] Celata, G.P., Cumo M., McPhail, S.J., and Zummo G., "Single-phase laminar and turbulent heat transfer in smooth and rough microtubes", *Journal of microfluid and nanofluid*, 3, pp. 697-707, **2007.**

[30] Morini, G.L., "Single-phase convective heat transfer in microchannels: a review of experimental results", *International Journal of Thermal Sciences*, 43, pp. 631-651, **2004.**

[31] Hetsroni, G., Mosyak, A., Pogrebnyak, E., and Yarin, L.P., "Fluid flow in micro-channels", *International Journal of Heat and Mass Transfer*, 48, pp. 1982-1998, **2005.**

[32] Lee, P., and Garimella S.V., "Thermally developing flow and heat transfer in rectangular microchannels of different aspect ratio", *International Journal of Heat and Mass Transfer*, 49, pp. 3060-3067, **2006.**

[33] Morini, G.L., "Laminar-to-Turbulent flow transition in microchannels", *Microscale Thermophys. Eng.*, 8, pp. 15-30, **2004.**

[34] Obot, N.T., "Toward a better understanding of friction and heat/mass transfer in microchannels-a literature review, *Microscale Thermophys. Eng.*, 6, pp. 155-173, **2002.**

[35] Choi, S.B., Barron, R.F., and Warrington, R.O, "Fluid flow and heat transfer in microtubes in: *Micromechanical Sensors, Actuators and Systems*, ASME DSC, Atlanta, GA, pp. 123-134, **1991.**

[36] Baviere, R., Favre-Marinet, M., and Le Person, S., "Bias effect on heat transfer measurements in microchannel flows", *International Journal of Heat and Mass Transfer*, 49, pp. 3325-3337, **2006.**

[37] Caney, N., Marty, P., and Bigot, J., "Friction losses and heat transfer of single-phase flow in a mini-channel*", Applied Thermal Engineering*, 27, pp. 1715-1721, **2007.**

[38] Rands, C., Webb, B.W., and Maynes, D., "Characterization of transition to turbulence in microchannels", *International Journal of Heat and Mass Transfer*, 49, pp. 2924-2930, **2006.**

[39] Ghiaasiaan, S.M., and Laker, T.S., "Turbulent forced convection in microtubes", *International Journal of Heat and Mass Transfer*, 44, pp. 2777-2782, **2001.**

[40] Hao, P-F., Zhang, X-W., Yao, Z-H., and He, F., "Transitional and turbulent flow in a circular microtube", *Experimental Thermal and Fluid Science*, 32, pp. 423-431, **2007.**

[41] Adams, T.M, Dowling, M.F., Abdel-Khalik, S.I., and Jeter, S.M., "Applicability of traditional turbulent single-phase forced convection correlations to non-circular microchannels", *International Journal of Heat and Mass Transfer*, 42, pp. 4411-4415, **1999.**

[42] Yang, W-H., Zhang, J-Z., and Cheng, H.E., "The study of flow characteristics of curved microchannel", *Applied Thermal Engineering*, 25, pp. 1894-1907, **2005.**

[43] Shen, S., Xu, J.L., Zhou, J.J., and Chen, Y., "Flow and heat transfer in microchannels with rough wall surfaces", *Energy Conversion and Management*, 47, pp. 1311-1325, **2006.**

[44] Mishan, Y., Mosyak, A., Pogrebnyak, E., and Hetsroni, G., "Effect of developing flow and thermal regime on momentum and heat transfer in micro-scale heat sink", *International Journal of Heat and Mass Transfer*, 50, pp. 3100-3114, **2007.**

[45] Koşar, A., Kuo C. J., and Peles, Y., "*Boiling heat transfer in rectangular microchannels with reentrant cavities*", International Journal of Heat and Mass Transfer, 48, pp. 4867-4886, **2005.**

[46] Huh, C., and Kim, H. M., "An experimental investigation of flow boiling in an asymmetrically heated rectangular microchannel", *Experimental Thermal and Fluid Science*, 30, pp. 775-784, **2006.**

[47] Lee, P.S., and Garimella, S.V., "Saturated flow boiling heat transfer and pressure drop in silicon microchannel arrays", *International Journal of Heat and Mass Transfer*, 51, pp. 789-806, **2008.**

[48] Thome, J.R., "*Boiling in microchannels: a review of experiment and theory*", International Journal of Heat and Fluid Flow, 25, pp. 128-139, **2004.**

[49] Wang, G., and Cheng, P., "An experimental study of flow boiling instability in a single microchannel", *International Communications in Heat and Mass Transfer*, 35, pp. 1229-1234, **2008.**

[50] Bogojevic, D., Sefiane, K., Walton, A.J., Lin, H., and Cummins, G., "Two-phase flow instabilities in a silicon microchannels heat sink", *International Journal of Heat and Fluid Flow*, 30, pp. 854-867, **2009.**

[51] Kandlikar, S.G., Shoji, M., and Dhir, V.K., Handbook of Phase Change, *Taylor & Francis*, USA, Chapter 15, pp. 376, **1999.**

[52] Qiu, Y.H., and Liu, Z.H., "Critical Heat flux in saturated and subcooled boiling for R-113 jet impingement on the stagnation zone", *Applied Thermal Engineering*, 25, pp. 2367-2378, **2005**.

[53] Lee, C.H, and Mudawar, I., "A mechanistic critical heat flux model for subcooled flow boiling based on local bulk flow conditions", *International Journal of Multiphase Flow*, 14, pp. 711-728, **1988**.

[54] Lee, J., and Mudawar, I., "Critical heat flux for subcooled flow boiling in micro-channel heat sinks", *International Journal of Heat and Mass Transfer*, 52, pp. 3341-3352, **2009**.

[55] Liu, W., Nariai, H., and Inasaka, F., "Prediction of critical heat flux for subcooled flow boiling", *International Journal of Heat and Mass Transfer*, 43, pp.3371-3390, **2000.**

[56] Wang, G., and Cheng, P., "Subcooled flow boiling and microbubble emission boiling phenomena in a partially heated microchannel", *International Journal of Heat and Mass Transfer*, 52, pp.79-91, **2009.**

[57] Haynes, B.S., and Fletcher, D.F., "Subcooled flow boiling heat transfer in narrow passages", *International Journal of Heat and Mass Transfer*, 46, pp. 3673-3682, **2003.**

[58] Callizo, C.M., Palm, B., and Owhaib, W., "Subcooled flow boiling of R-134a in vertical channels of small diameter", *International Journal of Multiphase Flow*, 33, pp. 822-832, **2007.**

[59] Collier, J.G., and Thome, J.R., Convective Boiling and Condensation, *Oxford Science Publications*, UK, Chapter 5, pp. 203, **2001.**

[60] Ghiaasiaan, S.M., Two Phase Flow Boiling and Condensation in Conventional and Miniature System, *Cambridge University Press*, UK, Part II, pp. 348, **2008.**

[61] Celata, G.P., Cumo, M., Guglielmi, M., and Zummo, G., Experimental investigation of hydraulic and single phase heat transfer in 0.130mm capillary tube, in: G.P. Celata, et al. (Eds.), *Proceedings of International Conference on Heat Transfer and Transport Phenomena in Microscale*, Begell House, New York, USA, pp. 108–113, **2000.**

[62] Shah, R.K., and Sekulic, D.P., Fundamentals of Heat Exchanger Design, *John Wiley&Sons*, pp. 502-506, **2003.**

[63] Kline, S., and McClintock, F.A., Describing Uncertainties in Single-Sample Experiments, *Mech. Eng. (Am. Soc. Mech. Eng.)*, 75, pp. 3-8, **1953.**

[64] Steinke, M.E., and Kandlikar, S.G., Single-phase liquid friction factors in microchannels, *International Journal of Thermal Sciences*, 45, pp. 1073-1083, **2006.**

[65] Rohsenow, W.M., Heat transfer with evaporation, *A Symposium Held at the University of Michigan During the Summer of 1952,* Univ. of Michigan Press, pp. 101-150, **1953.**